

Rates and Patterns of Groundwater Flow in the Cascade Range Volcanic Arc, and the Effect on Subsurface Temperatures

S. E. INGBRITSEN

U.S. Geological Survey, Menlo Park, California

D. R. SHERROD

U.S. Geological Survey, Vancouver, Washington

R. H. MARINER

U.S. Geological Survey, Menlo Park, California

The central Oregon section of the Cascade Range volcanic arc is characterized by relatively high Quaternary volcanic extrusion rates and hot-spring discharge rates, and by high conductive heat flow. However, a large area of near-zero near-surface conductive heat flow occurs in the younger volcanic rocks, due to downward and lateral flow of cold groundwater. Alternate models for the high heat flow observed in older rocks on the flanks of the Cascade Range involve (1) a laterally extensive midcrustal heat source or (2) a narrower, spot-tier deep heat source that is confined to the Quaternary arc and is flanked by relatively shallow conductive heat flow anomalies caused by regional groundwater flow. We simulated groundwater flow and heat transport through two cross sections west of the Cascade Range crest: one in the Breitenbush area, where there is no major arc-parallel normal faulting, and one in the McKenzie River drainage, where major graben-bounding faults exist. Measured temperature profiles, hot-spring discharge rates, and geochemical inferences constrain the results. The numerical simulations provide some estimates of regional-scale permeabilities; simulated bulk permeabilities of $\sim 10^{-14}$ m² in the youngest (0-2.3 Ma) rocks and $\sim 10^{-17}$ m² in the oldest (18-25 Ma) rocks allow the thermal observations to be matched. In general, permeability decreases downsection, but for rocks of any age, permeability at very shallow (<50 m) depths is probably much higher than the bulk permeability values required by the thermal observations: this is indicated by high recharge rates in 0-7 Ma rocks (>1 m yr⁻¹) and well-test data from domestic wells in rocks older than 7 Ma (which indicate permeability values of about 10^{-14} to 10^{-12} m²). In the simulations, the alternate conceptual models for the deep thermal structure were represented as wide or localized deep heat sources. We found that either model can satisfy the observations. Thermal observations in the Breitenbush area seem to require significant advective heat transfer, whereas the sparser observations in the McKenzie River area can be satisfied with either advection- or conduction-dominated simulations. Available regional gravity, magnetic, and electrical geophysical data do not clearly favor either of the two alternate models. Deep drilling in areas of high heat flow in the older rocks would be the most definitive test. The actual thermal structure is probably more complex than either of the models considered here.

INTRODUCTION

This report focuses on the hydrothermal systems of the Cascade Range in north-central Oregon; the study area includes a 135-km-long section of the arc between latitudes 44° 00' and 45° 15' N. It lies generally southeast of Portland, northeast of Eugene, and northwest of Bend and includes parts of the Cascade Range, Deschutes-Umatilla Plateau, and High Lava Plains physiographic provinces (Figure 1).

The Cascade Range is a 1200-km-long volcanic arc that extends from southern British Columbia to northern California. High-temperature igneous-related geothermal resources are assumed to exist in the Cascade Range [e.g., Brook *et al.*, 1979], but their magnitude and extent are poorly known. Several lines of evidence suggest relatively high geothermal potential in the central Oregon Cascade Range, a part of the arc characterized by relatively high volcanic extrusion rates [Sherrod and Smith, 1990], hot-spring discharge rates [Mariner *et al.*, 1990], and conductive heat flow [Blackwell *et al.*, 1982, 1990a; Blackwell and Steele, 1987; Blackwell and Baker, 1988b]. The central

Oregon Cascade Range also includes several silicic volcanic systems that are probably sufficiently large and young enough to retain significant amounts of heat [Smith and Shaw, 1975, 1979]. Extrusion rates and hot-spring discharge rates decrease north and south of the area, and conductive heat flow decreases to the north and possibly to the south.

Two conceptual models of the thermal structure of the north-central Oregon Cascades are shown in Figure 2. These contrasting models have significant implications for magmatism and geothermal resource potential in the Cascade Range. One model invokes a relatively narrow, spatially variable deep heat flow anomaly that expands laterally at shallow depths because of groundwater flow (Figure 2a). We refer to this as the lateral-flow model. The lateral-flow model is similar to two of the models for the Western Cascade hot springs presented by Blackwell *et al.* [1982, Figure 10, models 2 and 3], except that we suggest significant spatial variability in the heat source. Another model invokes an extensive midcrustal heat source underlying both the Quaternary arc and adjacent older rocks (Figure 2b) [Blackwell *et al.*, 1982; Blackwell and Steele, 1983, 1985]. The thermal effects of hydrothermal circulation may be locally superimposed on the effects of this extensive midcrustal heat source [Blackwell and Steele, 1987; Blackwell and Baker 1988a, b; Blackwell *et al.*, 1990a], which is envisioned as a long-lived

This paper is not subject to U.S. copyright. Published in 1992 by the American Geophysical Union.

Paper number 91JB03064.

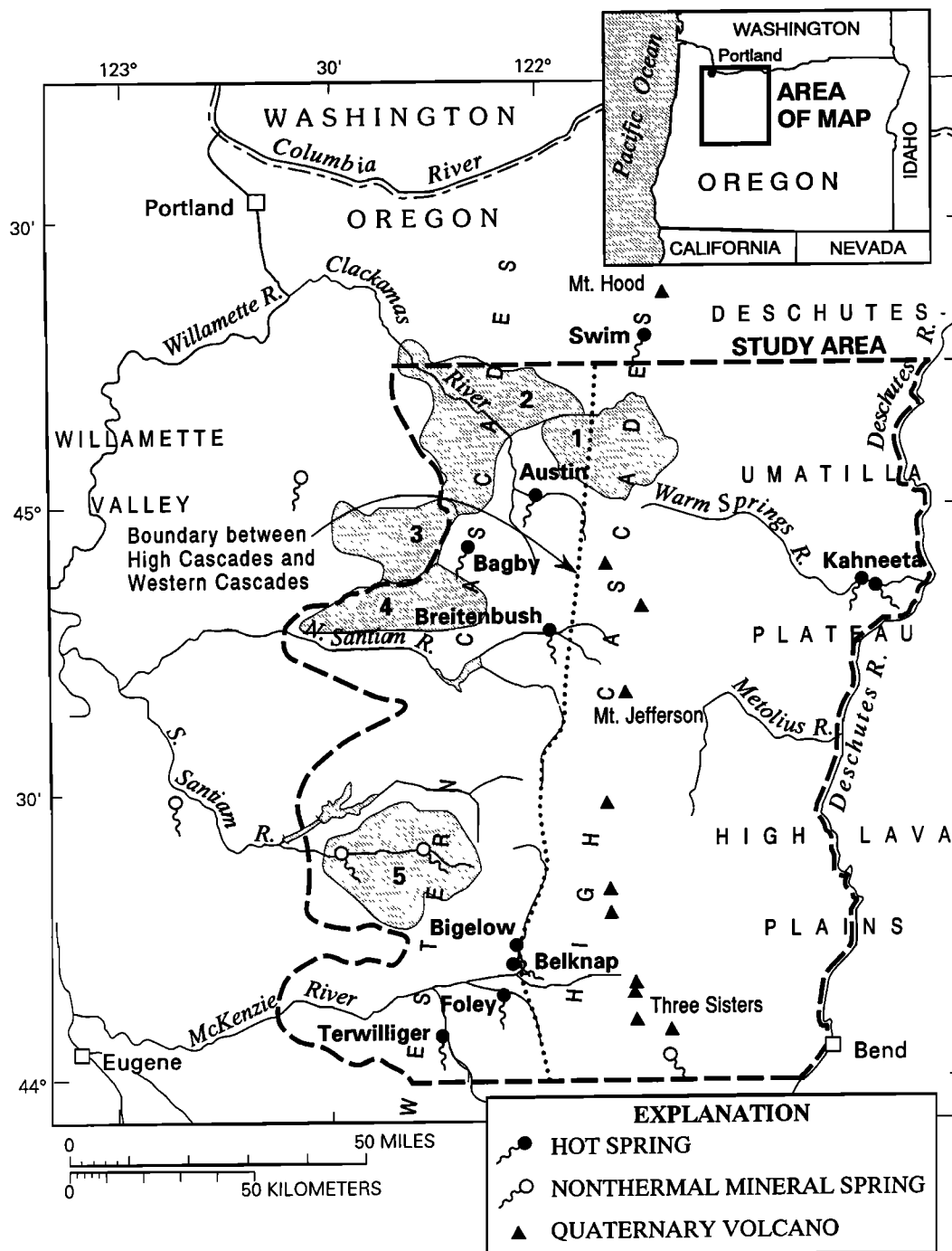


Fig. 1. Location of the study area in north-central Oregon and location of basins for which groundwater recharge is estimated. Physiographic provinces from Baldwin [1976], High Cascades-Western Cascades boundary (dotted line) from Callaghan [1933, Figure 1]. Drainage basins are 1, Oak Grove Fork Clackamas River; 2, Clackamas River between Three Lynx and Estacada; 3, Molalla River; 4, Little North Santiam River; and 5, South Santiam River.

zone of magma interception, storage, and crystallization with a time-averaged temperature of about 600 °C [Blackwell *et al.*, 1990b, p. 19,514]. Though the actual thermal structure is probably more complex than either of the simple models shown in Figure 2, they provide useful end-members for discussion. The numerical simulations discussed here illustrate some of the implications of each model.

HYDROGEOLOGIC SETTING

The Cascade Range in Oregon is customarily divided into two physiographic subprovinces, the relatively uneroded High Cascades and the deeply dissected Western Cascades [Callaghan and Buddington, 1938]. That distinction is useful here because of the fundamental control that topography exerts

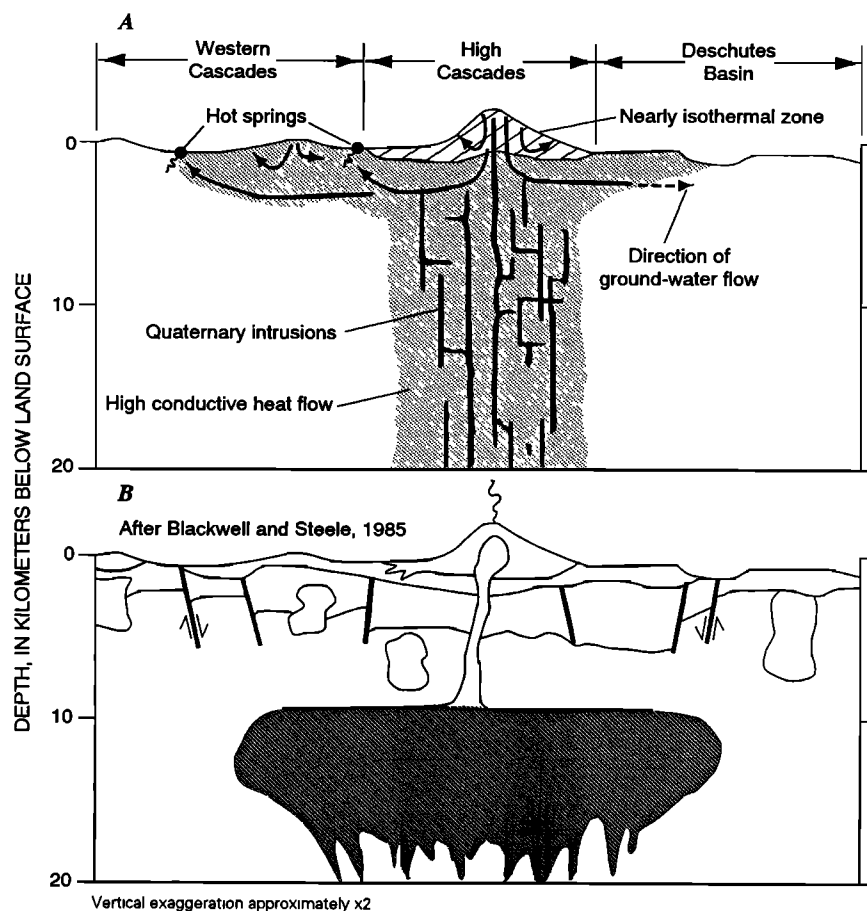


Fig. 2. (a) Conceptual model of the thermal structure of the north-central Oregon Cascades, showing magmatic heat sources beneath the Quaternary arc. (b) The laterally extensive midcrustal heat source proposed in other studies [e.g., Blackwell *et al.*, 1982, 1990a; Blackwell and Steele, 1983, 1985].

on regional hydrology. The High Cascades subprovince forms the crest of the range and is built mainly of permeable upper Pliocene and Quaternary volcanic rocks that create a broad ridge receiving heavy snowfall. The High Cascades are a regional groundwater recharge area; about half of the incident precipitation infiltrates and recharges ground-water systems. In contrast, the Western Cascades is a deeply incised terrain underlain by less permeable Oligocene to lower Pliocene volcanic and volcanoclastic strata. Topographically driven groundwater flow from the High Cascades feeds springs to the west and east.

We emphasize Quaternary (0-2 Ma) volcanic rocks (Figures 3, 5, 6, 8, 15, 21) not because of any major structural or stratigraphic break but because active high-temperature hydrothermal systems are often related to Quaternary magmatism. Quaternary silicic rocks are of particular interest because silicic magmas are probably erupted from storage chambers in the upper continental crust, whereas basic magmas generally do not form large high-level storage chambers [Smith and Shaw, 1975]. Quaternary dacite and rhyolite are confined to the Mount Jefferson area and the area between Three Sisters and Bend (Figure 1).

The Cascade Range forces generally west-to-east-moving air masses to ascend and release moisture. Average annual precipitation in the study area ranges from more than 2.5 m in parts of the Western and High Cascades to less than 0.25 m along the lower Deschutes River [U.S. Department of Agriculture, Soil

Conservation Service, 1964]. Precipitation decreases abruptly east of the Cascade Range crest.

Groundwater Recharge

Late-summer stream discharge (baseflow) in the Cascade Range is composed almost entirely of groundwater contributions. The unit baseflow (baseflow per unit area), an index of groundwater recharge, has been estimated for five basins west of the Cascade Range crest (Figure 1), using baseflow estimates from low-flow values for the period 1981-1985 [U.S. Geological Survey, 1983a, b, 1984, 1986, 1987]. During this time annual runoff in the Willamette River basin ranged from 83 to 130% of the long-term mean value. The late-summer baseflow is a minimum estimate of the groundwater contribution to streamflow, which may be considerably larger in fall, winter, and spring.

The estimated recharge rates show a rough inverse correlation with the age of rocks exposed in the basin (Table 1). They vary by more than an order of magnitude, ranging from $1 \times 10^{-9} \text{ m s}^{-1}$ in the 17-25-Ma rocks of the South Santiam basin (Figure 1, area 5) to $26 \times 10^{-9} \text{ m s}^{-1}$ in the 0-7 Ma rocks of the Oak Grove Fork basin (area 1). The relatively low recharge rate calculated for the South Santiam basin is ~1% of the local annual precipitation; the infiltration rate for the Oak Grove Fork basin represents ~47% of the annual precipitation.

TABLE 1. Estimated Minimum Groundwater Recharge Rates for Selected Basins West of the Cascade Range Crest

Basin	Area, m ² x 10 ⁸	Dominant Lithology	Minimum Groundwater Recharge, ^a m s ⁻¹ x 10 ⁻⁹
Oak Grove Fork Clackamas River ^b	3.3	<7 Ma andesite	26
Clackamas River between gaging stations 14209500 and 14210000	5.0	7-17 Ma andesite	4.9 ^c
Molalla River	2.5	7-17 Ma andesite (volcanic diamicton)	3.7
Little North Santiam River	2.9	17-25 Ma andesite	4.2
South Santiam River	4.5	17-25 Ma andesite	1.1 ^c

See Figure 1 for basin locations.

^a Baseflow per unit area.

^b Stream flow at U.S. Geological Survey gaging station 14209000 was adjusted for changes in storage at Timothy Lake.

^c Estimated rate for >7 Ma rocks only, obtained by assuming that the unit baseflow for the <7 Ma rocks in the basin is the same as that calculated for the Oak Grove Fork basin (26 x 10⁻⁹ m s⁻¹).

The inverse correlation between recharge rate and age of rocks probably reflects reduced primary porosity and permeability in the older volcanic rocks; the relatively steep topography in areas where older rocks are exposed may also tend to reduce infiltration. We believe that reduced permeability is the more important factor, because conductive heat flow data (discussed

below) also support the inference that the older rocks are much less permeable.

Hot Springs

Hot springs in the study area discharge from rocks older than about 7 Ma at elevations of 440-680 m. Most are found near

TABLE 2. Chemical Composition, Geothermometer Temperatures, and Discharge Data for Hot Springs in the Study Area

Hot Spring	pH	Ca	Mg	Na	K	HCO ₃	Cl	Br	SO ₄	SiO ₂	T _d ^a	T _g ^b	Q _v ^c L s ⁻¹	³ He/ ⁴ He, ^d R/R _a
Austin	7.4	35	0.10	305	6.4	36	390	1.2	130	81	86	186	120±6	5.7
Bagby	9.4	3.3	<0.05	53	0.7	69	14	-	42	74	58	52	1	1.2
Breitenbush	7.0	95	1.1	745	31	137	1200	4.2	140	163	84	174	13±2	6.5
Bigelow	7.8	195	0.53	675	15	22	1250	3.8	140	73	59	155	-	-
Belknap	7.6	210	0.34	660	15	20	1200	3.9	150	91	73	152	20±3 ^e	-
Foley	8.0	410	0.08	555	8.7	20	1350	4.0	510	63	79	100	11±4	-
Terwilliger	8.5	215	0.07	405	6.1	21	790	2.2	240	47	46	135	5	-
Kahneeta	8.1	13	0.05	400	11	603	240	0.8	31	78	83	137	50±5	-

Dashes indicate the absence of data. pH in standard units. Temperatures (T) are in degrees Celsius (°C). Concentrations are in milligrams per liter (mg L⁻¹). Cations were determined by inductively coupled plasma, bicarbonate by acid titration, chloride by colorimetry or mercurimetric titration, bromide by ion chromatography, sulfate by turbidimetry, and silica by atomic absorption and molybdate blue.

^a Discharge temperature.

^b Chemical geothermometer temperatures based on anhydrite saturation, except for Kahneeta and Bagby, which are based on the silica (quartz) and cation geothermometers. The solubility of anhydrite (CaSO₄) provides a geothermometer which indicates maximum temperature [Ellis and Mahon, 1977]. Anhydrite-saturation values for the Na-Cl and Na-Ca-Cl waters that discharge in the Western Cascades correlate well with sulfate-water isotope temperatures (R. H. Mariner et al., unpublished manuscript, 1992). The temperatures listed for Kahneeta and Bagby are averages of the quartz and cation geothermometers. These and other geothermometers are discussed by Fournier [1981].

^c Discharge based on chloride-flux measurements, except for Bagby Hot Spring, where discharge was measured directly. Error bars are based on the standard deviation of replicate measurements.

^d ³He/⁴He ratio (R) normalized by the atmospheric ratio (R_a). Unpublished data provided by Peggy O'Brien Dickinson of Woods Hole Oceanographic Institution.

^e Combined discharge of Bigelow and Belknap Hot Springs.

major streams that originate in the Quaternary arc, in deeply incised valleys that focus the discharge from regional groundwater flow systems. The location of hot springs within a relatively narrow elevation range implies that topography is a major control on thermal-water discharge. In the study area no hot springs are found in the High Cascades.

The discharge rates of hot springs in the study area (Table 2) were determined on the basis of increases in the Na and Cl loads of nearby streams [Mariner et al., 1990]. Recent repeated determinations in our study area allowed us to compare several solute-inventory methods and to assess the reproducibility of the results [Ingebritsen et al., 1991].

Total hot-spring discharge in the study area ($220 \pm 20 \text{ L s}^{-1}$) amounts to less than 0.2% of the estimated groundwater

recharge in the Quaternary arc ($>1 \times 10^5 \text{ L s}^{-1}$, based on an estimated recharge rate of $>26 \times 10^9 \text{ m s}^{-1}$ (Table 1) and $\sim 4 \times 10^9 \text{ m}^2$ of Quaternary exposures in the study area). Samples collected 15-40 km downstream from the hot-spring groups failed to detect significant additional discharges of saline water, with the exception of samples from the U.S. Geological Survey streamflow-gaging station on the McKenzie River east of Vida [Ingebritsen et al., 1991].

PATTERNS OF GROUNDWATER FLOW

The shallow nonthermal groundwater is commonly mixed cation-bicarbonate water. Concentrations of total dissolved solids reflect the copious groundwater recharge in the High Cascades, ranging from less than 100 mg L^{-1} in the High Cascades

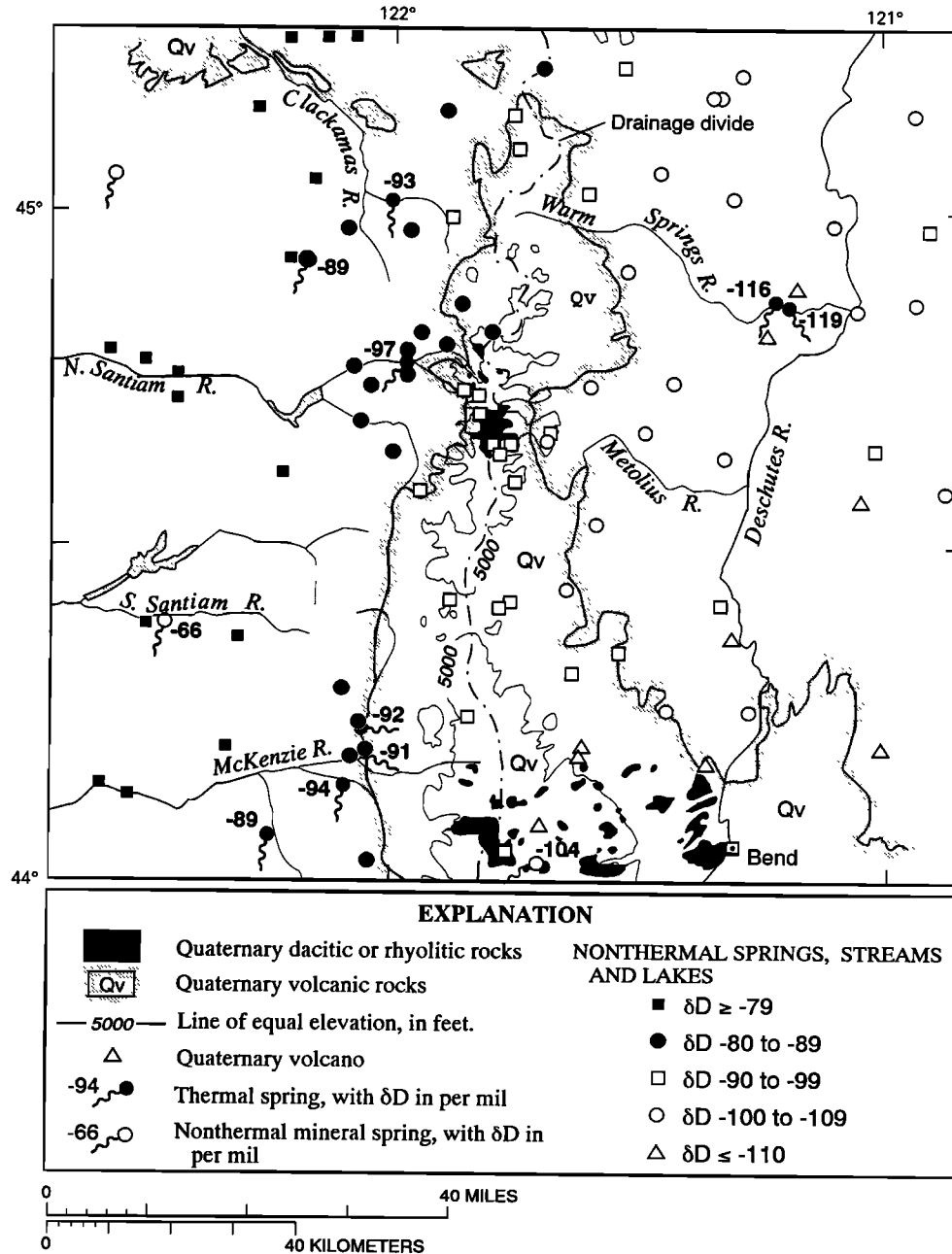
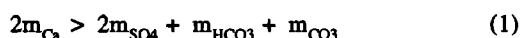


Fig. 3. Deuterium content of waters sampled in and near the study area, selected elevation contours, and distribution of Quaternary volcanic rocks.

to about 300 mg L⁻¹ elsewhere in the study area. Relatively saline nonthermal groundwater (>300 mg L⁻¹ dissolved solids) occurs only near the western and eastern boundaries of the study area (Figure 1), in parts of the Western Cascades where 25-35 Ma sedimentary rocks are exposed and in the lower Deschutes basin [Ingebritsen *et al.*, 1988, 1991]. In general the nonthermal waters are very different chemically from the thermal waters of the study area, most of which are Na-Cl or Na-Ca-Cl waters with dissolved solids concentrations ranging up to about 3,000 mg L⁻¹. The Na-Ca-Cl waters have sodium and chloride as the dominant cation and anion, but they also have the peculiar characteristic that some of the calcium (Ca⁺²) present is electrically balanced by chloride (Cl⁻¹) [Hardie, 1983]. That is,



where *m* is in molal units (moles solute/1000 grams water). Nonthermal Na-Cl and Na-Ca-Cl waters were sampled from a few wells drilled into 25-35 Ma sedimentary rocks near the western edge of the study area and are commonly encountered southwest of the study area in interlayered volcanic and sedimentary rocks of the lower Eocene marine Umpqua Formation [e.g., Robison, 1974; Robison and Collins, 1977; Frank, 1979]. However, stable-isotope data [Ingebritsen *et al.*, 1988, 1991] clearly indicate that these waters are of local origin.

In contrast, the isotopic composition of thermal waters in the Western Cascades suggests that they were recharged at relatively high elevations. Deuterium (δD) data from waters sampled at 127 sites in and near the study area are plotted in Figure 3. The deuterium values vary systematically from about -65 ‰ near the western edge of the study area to less than -115 ‰ east of the Three Sisters and near the Deschutes River (Figure 3). Corresponding δ¹⁸O values range from about -9 to -15 ‰.

Figure 4 shows the relation between δD and elevation for thermal and nonthermal waters sampled west of the Cascade Range crest. The nonthermal data are from low-salinity (<70 mg L⁻¹ Na) springs and wells in unchanneled or headwater drainage basins, and presumably represent local meteoric water. They show a strong inverse correlation between δD and elevation.

On the basis of a linear-least-squares fit to the nonthermal data, the range of δD values measured in the thermal waters (-97 to -89 ‰) is best matched by that of meteoric waters at elevations of 1350-1850 m (Figure 4). Only very limited areas outside the Quaternary arc attain such elevations. Extensive areas at elevations above 1500 m (~5000 feet) are found only in the highlands around Mount Jefferson and the Three Sisters (Figure 3). Since the hot springs in the Western Cascades are at elevations of 490-680 m, a significant elevation difference is available to drive the thermal circulation systems. The average topographic gradient between the inferred recharge areas and the hot springs is as large as 0.1.

It is arguable that the Western Cascade thermal waters are local meteoric waters, but that the isotopic composition of precipitation has changed significantly since they were recharged. This could be the case if the thermal waters were recharged in the Pleistocene. The average thermal water contains about 17 ‰ less deuterium than average meteoric water at the same elevation (Figure 4). No paleotemperature data are available for the Cascade Range, but a decrease of about 3-4 °C in mean an-

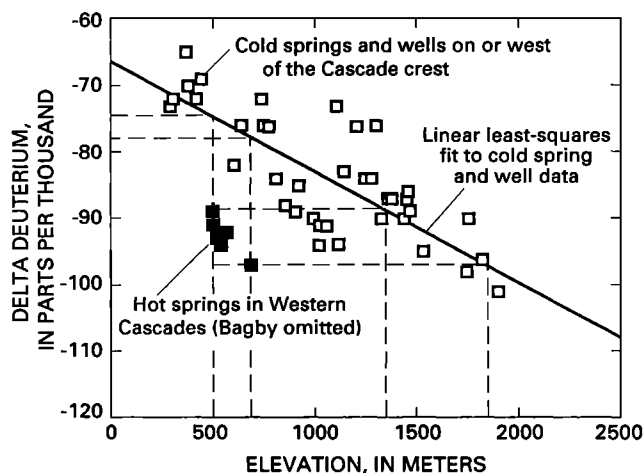


Fig. 4. Relation between deuterium content (δD) and elevation for waters on or west of the Cascade Range crest. Solid squares are from Na-Cl and Na-Ca-Cl thermal waters in the Western Cascades. Open squares are nonthermal samples from low-salinity springs and wells in unchanneled or headwater basins, and represent local meteoric water. Line is least squares fit to the nonthermal water data. Values for δ¹⁸O show a similar pattern because the oxygen shift of the thermal waters is minimal (-1 ‰).

nual air temperature would probably be sufficient to decrease the deuterium content of precipitation by 17 ‰ [Dansgaard, 1964; Gat, 1980].

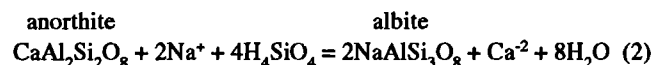
Because the Na-Cl and Na-Ca-Cl hot springs in the Western Cascades are located at sites expected to capture regional groundwater flow from the Quaternary arc, we prefer to explain the isotopic composition of these thermal waters in terms of higher-elevation recharge during the Holocene. Relatively high ³He/⁴He ratios (Table 2) are further suggestive evidence that the thermal waters originate in areas of Quaternary volcanism, and high rates of hot-spring heat transport (discussed below) are difficult to explain in terms of local circulation.

THERMAL WATERS

Breitenbush Hot Springs and the hot springs in the McKenzie River drainage (Bigelow, Belknap, Foley, and Terwilliger) discharge Na-Ca-Cl waters, and Austin Hot Springs discharges Na-Cl waters (Table 2). Bagby Hot Springs discharges dilute Na-mixed anion waters and is also unique among the Western Cascade hot springs in that it is isolated from the Quaternary arc by major drainage divides. This location, chemical composition, and a relatively low ³He/⁴He ratio (Table 2) suggest that Bagby is the product of relatively local deep circulation. The Na-HCO₃ waters of Kahneeta Hot Springs are also markedly different from other thermal waters in the study area.

The definition of Na-Ca-Cl waters (Eq. 1) implies that at least part of the Ca²⁺ is electrically balanced by Cl⁻. The presence of a CaCl₂ component is an unusual chemical signature shared by many rift-zone hydrothermal brines [Hardie, 1983]. In North America, thermal Na-Ca-Cl waters occur primarily in the Salton Trough and in the Columbia embayment, which encompasses northwest Oregon and southwest Washington and may be built on Cenozoic oceanic crust [Hamilton and Myers, 1966].

Hardie [1983] demonstrated that the Na-Ca-Cl waters of the Reykjanes, Iceland, system probably develop from Na-Cl waters by albitization of plagioclase:



where anorthite represents the calcium component of intermediate plagioclase. The resulting increase in dissolved calcium causes precipitation of calcite (CaCO_3) and anhydrite (CaSO_4). Calcite precipitation can lead to very low HCO_3^- concentrations (Table 2), unless a source of CO_2 is present. Another possible control on Na/Ca ratios in Na-Ca-Cl waters is conversion of plagioclase or Ca-bearing zeolites to analcime ($\text{NaAlSi}_2\text{O}_6 \cdot \text{H}_2\text{O}$) (R. H. Mariner et al., unpublished manuscript, 1992). In either case, Na-Ca-Cl thermal waters can be regarded as having evolved from Na-Cl waters by alteration of a Ca-bearing mineral.

Sources of Chloride

Mariner et al. [1980] and Ingebritsen and Sorey [1985] suggested that Na-Cl and Na-Ca-Cl thermal waters of the Cascade Range obtain high concentrations of Na and Cl by circulating through rocks deposited in a marine environment. However, Conrey and Sherrod [1988] described xenoliths from the Cascade Range that appear to have lost Na and Cl during recrystallization to quartz, potassium feldspar, and illite and suggested that the source of these constituents in the thermal waters could be altered volcanic glass. Mariner et al. [1989] noted that Br/Cl weight ratios in the thermal waters (Table 2) are similar to those in sea water (3.5×10^{-3}) rather than volcanic ash (1.5×10^{-3} for Mount St. Helens ash) and again suggested a "marine" Cl source. However, the Br/Cl ratio in Japanese volcanic rocks varies within a range that brackets the sea-water ratio (1.6×10^{-3} [Brehler and Fuge, 1978]).

Mass-balance considerations suggest the presence of a source of chloride in addition to the volcanic rocks. The chlorine contents of Cascade Range volcanic rocks are highly variable and poorly known, but probably quite low. H.N. Elsheimer (written communication, 1990) obtained a mean value of 160 mg kg^{-1} for 9 samples of Eocene or younger volcanic rocks. Complete leaching of Cl from about $70 \text{ km}^3/\text{km arc length/m.y.}$ of volcanic rocks with an average Cl content of 160 mg kg^{-1} would be required to supply the current flux of chloride from hot springs (about 120 g s^{-1} (Table 2) distributed over the 135 km of arc length in the study area). This rate is more than an order of magnitude greater than the long-term volcanic production rate of $3\text{-}6 \text{ km}^3/\text{km arc length/m.y.}$ [Sherrod and Smith, 1990].

The most probable sources of chloride are marine rocks and magmatic volatiles. Lower and middle Eocene (~44-58 Ma) marine rocks likely extend beneath the study area, because they are exposed in the Coast Range to the west [Wells and Peck, 1961] and at the Hay Creek anticline ~70 km east of Mount Jefferson [Wareham, 1986]. A magmatic source also seems feasible: relatively high $^3\text{He}/^4\text{He}$ values for the Na-Ca-Cl thermal waters (Table 2) indicate that some dissolved constituents are of magmatic origin, and most magmatic chloride will partition to an aqueous phase. If we assume conservatively that the Cl content of the magma is 0.1 weight percent [Burnham, 1979], an intrusion rate of $10 \text{ km}^3/\text{km arc length/m.y.}$ could supply the current flux of Cl from the hot-spring systems of the study area (~1 g s^{-1} per km arc length). This intrusion rate is within the range of rates ($9\text{-}33 \text{ km}^3/\text{km arc length/m.y.}$) calculated by Ingebritsen et al. [1989, 1991] on a heat-budget basis.

Geothermometry

The commonly used quartz [Fournier and Rowe, 1966], cation (Na-K-Ca [Fournier and Truesdell, 1973]), and $\text{SO}_4\text{-H}_2\text{O}$ isotope [Mizutani and Rafter, 1969] geothermometers give disparate results when applied to the Na-Cl and Na-Ca-Cl waters of the study area. Only for Breitenbush Hot Springs are all three geothermometers in reasonably good agreement (within 30°C). For the other Na-Cl and Na-Ca-Cl springs the Na-K-Ca temperatures are $45\text{-}84^\circ\text{C}$, the silica (quartz) temperatures are $99\text{-}132^\circ\text{C}$, and the $\text{SO}_4\text{-H}_2\text{O}$ temperatures are $136\text{-}181^\circ\text{C}$ (R. H. Mariner et al., unpublished manuscript, 1992).

The retrograde solubility of anhydrite can provide a geothermometer that indicates maximum temperature [Ellis and Mahon, 1977]. Because excess Ca is produced by alteration of plagioclase, the Na-Cl and Na-Ca-Cl thermal waters are likely to be saturated with anhydrite at depth. Calculated anhydrite saturation temperatures agree remarkably well with the $\text{SO}_4\text{-H}_2\text{O}$ temperatures of the Na-Cl and Na-Ca-Cl waters in the study area (to within about 10°C ; R. H. Mariner et al., unpublished manuscript, 1992). The $\text{SO}_4\text{-H}_2\text{O}$ and anhydrite geothermometers are completely independent, so their close agreement is good evidence that the temperatures estimated by these methods are correct.

The low temperature estimates yielded by the Na-K-Ca geothermometer may be due to the low Pco_2 of the Na-Cl and Na-Ca-Cl waters and (or) to the elevated Ca concentrations. Pco_2 in these waters is much lower than in the waters from which the geothermometer was empirically derived, and the Na-K-Ca temperature of the relatively CO_2 -rich Breitenbush Hot Springs waters ($\text{Pco}_2 \sim 0.01$ bars) is about 70°C higher than those estimated for the other Na-Cl and Na-Ca-Cl waters ($\text{Pco}_2 \sim 0.001$ bars at the anhydrite saturation temperatures). The low silica geothermometers may reflect removal of silica by precipitation at or near the spring temperatures. The rates of $\text{SO}_4\text{-H}_2\text{O}$ exchange reactions are relatively slow, so the $\text{SO}_4\text{-H}_2\text{O}$ temperature is more likely to reflect equilibrium attained at depth.

In Table 2 we list anhydrite saturation temperatures for the Na-Cl and Na-Ca-Cl waters, and an average of the silica and Na-K-Ca temperatures for the Na-mixed anion (Bagby) and Na- HCO_3^- (Kahneeta) waters. For Bagby and Kahneeta the silica and Na-K-Ca temperatures are in good agreement. The anhydrite saturation temperatures are significantly higher, but these relatively low-Ca waters may never have been saturated with anhydrite.

Residence Times

There does not appear to be any absolute way to estimate residence times for the Western Cascade thermal waters. The precipitation of calcite that accompanies the evolution of Na-Ca-Cl waters precludes carbon-14 dating, as does the probable presence of magmatic sources of CO_2 . The high chloride content of the Western Cascade thermal waters would complicate chlorine-36 dating. However, residence times can be constrained indirectly on the basis of other geochemical indicators.

Our interpretation of stable-isotope data in terms of Holocene recharge suggests maximum residence times of about 10,000 years, and the kinetics of sulfate-water oxygen-isotope equilibration can be used to calculate minimum residence times for the Na-Cl and Na-Ca-Cl thermal waters. Calculated equilibration times for hot-spring waters of the study area range from 40 years (Austin Hot Springs) to 2000 years (Foley Springs).

The time required for equilibration decreases with increasing reservoir temperature and increases with increasing pH ($\log t = 2.54 [10^3 T] + b$), where t is the half time of exchange in hours, T is absolute temperature, and b is -1.17 at pH 7 and 0.25 at pH 8 [McKenzie and Truesdell, 1977]).

HOT-SPRING HEAT TRANSPORT

The geochemical evidence summarized above indicates that the thermal waters are recharged in the Quaternary arc; therefore the hot-spring systems transfer heat from the Quaternary arc to the older rocks on the flanks of the Cascade Range. One measure of the heat transported advectively by a hot-spring system is given by the product $A = Q_i \rho c (T_g - 5)$, where Q_i is the hot spring discharge (Table 2), ρ is fluid density, c is heat capacity of the fluid, T_g is a chemical geothermometer temperature (Table 2), and 5°C is the approximate mean temperature at the hot-spring recharge elevations inferred from the stable-isotope data. In this calculation it is appropriate to use T_g rather than the discharge temperature (Table 2, T_d) because the hot-spring waters cool conductively from T_g to T_d , without gaining volume by mixing with nonthermal waters. The good agreement between $\text{SO}_4\text{-H}_2\text{O}$ and anhydrite-saturation temperatures, low tritium levels in the hot-spring waters (R. H. Mariner et al., unpublished manuscript, 1992), and a strong correlation between discharge rate and discharge temperature (Table 2) rule out substantial near-surface mixing. The major sources of uncertainty in the heat-transport calculation are Q_i and T_g . The uncertainty in Q_i has been estimated from replicate measurements (Table 2), and T_g may be $\pm 10^\circ\text{C}$.

The total advective heat transport by hot-spring systems in the study area is thus 125-170 MW. The anhydrite-saturation temperatures listed in Table 2 give a value of 148 MW (Figure 5); substituting $\text{SO}_4\text{-H}_2\text{O}$ isotope temperatures (R. H. Mariner et al., unpublished manuscript, 1992) gives a similar value of 147 MW. These values are large enough to represent a significant component of the regional heat budget, as discussed by Ingebritsen et al. [1989, 1991]. They can be compared with the heat released by magmatic extrusion. The Quaternary magmatic extrusion rate of 3-6 km^3/km arc length/m.y. [Sherrod, 1986] represents an average heat release of 60 to 120 MW in the study area, assuming a basaltic magma with typical properties (initial temperature 1,200 $^\circ\text{C}$, latent heat of crystallization 420 J g^{-1} , specific heat 1.25 $\text{J g}^{-1} \text{ }^\circ\text{C}^{-1}$, and density 2.65 g cm^3 ; these values for a basaltic melt are taken from Jaeger [1964] and Harris et al. [1970]). A more pertinent comparison would be with the heat provided by magmatic intrusion, but intrusion rates and subsolidus temperatures can be inferred only within broad limits. Ingebritsen et al. [1989, 1991] derived a range of intrusion rates (9-33 km^3/km arc length/m.y.) from a heat-budget analysis. They invoked magmatic intrusion to explain a thermal input of 160 MW to the Quaternary arc. For the lower intrusion rate (9 km^3/km arc length/m.y.), this quantity of heat is supplied by the latent heat of crystallization plus 900 $^\circ\text{C}$ of magmatic cooling; for the higher limiting rate (33 km^3/km arc length/m.y.) it is supplied entirely by latent heat. The intrusion rates calculated by Ingebritsen et al. [1989, 1991] and cited here are lower than those calculated by Blackwell et al. [1990b], who proposed an intrusion rate of $\sim 55 \text{ km}^3/\text{km}$ arc length/m.y. for central Oregon. This is partly because Blackwell et al. [1990b] invoked a lower outer-arc "background" heat flow (45-50 mW m^{-2} versus 60 mW m^{-2}), but most of the discrepancy is due to their assumption that

lateral heat transfer by groundwater is negligible. Blackwell et al. [1990a, b] argue that the high heat flow values observed in rocks older than 7 Ma can reasonably be extrapolated to mid-crustal depths.

CONDUCTIVE HEAT FLOW

Conductive heat flow data indicate that the Quaternary arc and adjacent 2-7-Ma volcanic rocks constitute a large area of low-to-zero near-surface conductive heat flow resulting from downward and lateral flow of cold groundwater. In contrast, near-surface conductive heat flow is high ($>100 \text{ mW m}^{-2}$) in rocks older than ~ 7 Ma exposed at lower elevations in parts of the Western Cascades. A similar pattern of low-to-zero conductive heat flow in permeable volcanic highlands and relatively high heat flow in older, less permeable rocks at lower elevations was observed by Mase et al. [1982] in the Cascade Range of northern California.

The conductive heat flow data set for the study area was collected mostly by Blackwell et al. [1982], Black et al. [1983], Blackwell and Baker [1988b], and Ingebritsen et al. [1988], and was compiled in Ingebritsen et al. [1988, 1991]. The heat flow contours in Figure 6a indicate estimated conductive heat flow at the depths of conventional heat flow measurements (100-200 m). The contours were generated by a constrained inverse-distance-squared algorithm [Ingebritsen et al., 1991]. In five instances the contouring ignored changes in gradient found at depths greater than about 200 m (Figure 7). For example, site 87 (EWEB-CL of Blackwell et al. [1982]) was assigned a high heat flow on the basis of the high temperature gradient to ~ 205 m depth. The hydrologically controlled gradient disturbances observed in most of the deeper holes indicate that the actual crustal heat flow may be much different than the heat flow pattern defined by the shallow (<200 m) measurements.

Figure 6 compares our conductive heat flow contours with those of Blackwell et al. [1990a]. The contours shown east of the Cascade Range crest are based on a limited amount of low-quality data, and both sets are highly speculative. West of the Cascade Range crest, where more data are available, our contours are generally similar to those of Blackwell et al. [1990a]. There are two significant differences: (1) we identify a heat flow "trough" in the western part of the Western Cascades, and (2) we close the 100 mW m^{-2} contour against the Quaternary arc between the two hot-spring groups in the Western Cascades (the Austin-Breitenbush group and the McKenzie River group). The heat flow trough is suggested by data acquired by Ingebritsen et al. [1988]. Closing the 100 mW m^{-2} contour is consistent with the limited data available in the area between hot-spring groups. Blackwell et al. [1982, 1990a; Blackwell and Steele, 1983, 1985] explained the near-surface heat flow data in terms of an extensive midcrustal heat source underlying both the Quaternary arc and adjacent older rocks (Figure 2b). The edge of such a heat source would lie beneath the inflection point in surficial heat flow, or approximately below the 80 mW m^{-2} contour of Blackwell et al. [1990a] (Figure 6b), which is as far as 30 km west of the Quaternary arc. The data can alternatively be explained in terms of a narrower, spatially variable deep heat flow anomaly that expands laterally at relatively shallow depths because of groundwater flow (Figure 2a). This lateral-flow model attributes much of the high heat flow observed in the older rocks to hydrothermal circulation and thus predicts systematically lower heat flow values between the two hot-spring groups.

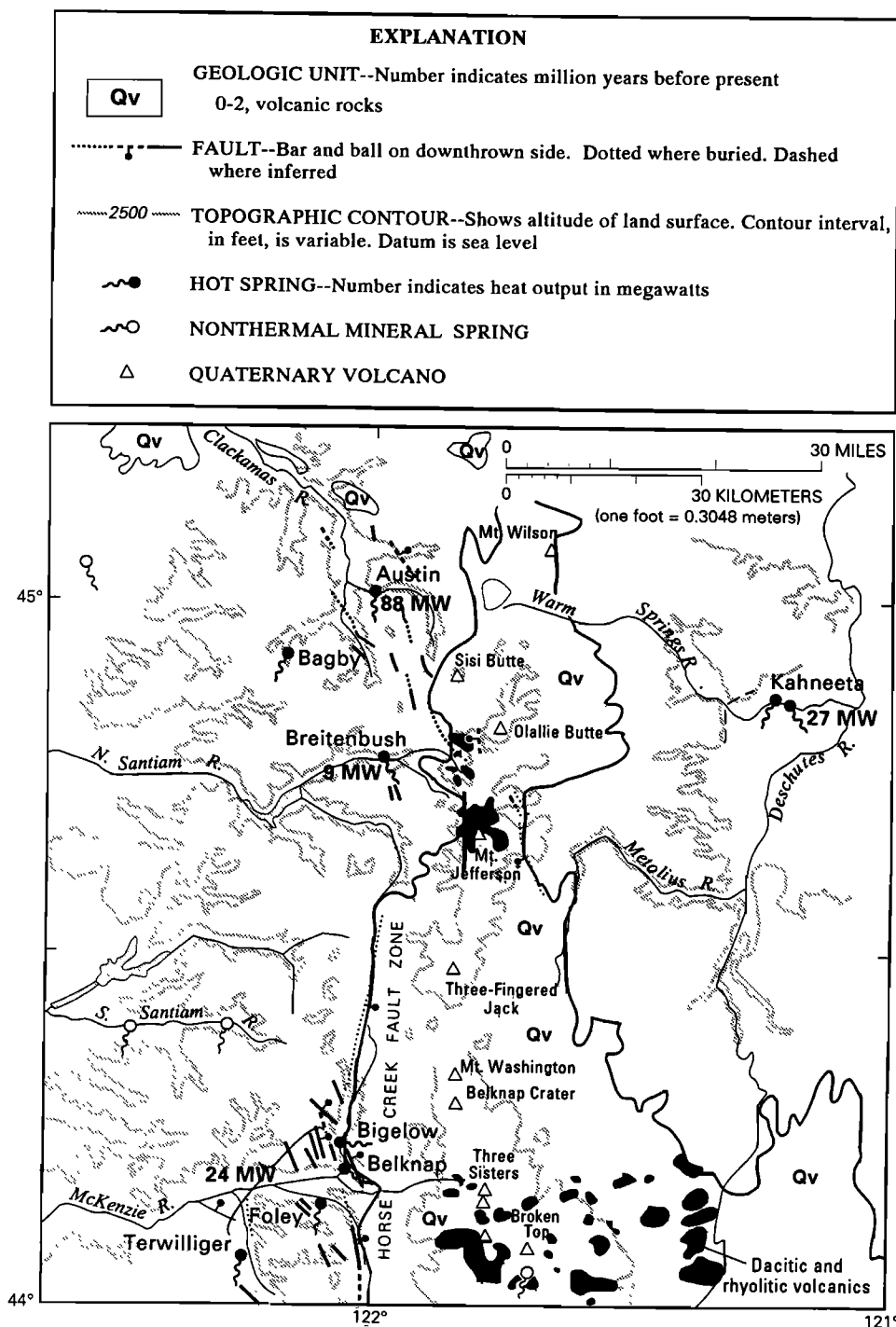


Fig. 5. Location of hot springs, generalized topography, selected geologic structures, Quaternary volcanic rocks, and the amount of heat transported advectively by the hot-springs systems. The total heat transported by hot springs in the McKenzie drainage (~24 MW) is 1.25 times the value obtained from the individual spring groups (Table 2), due to the diffuse input of thermal water into the surface drainage. Geologic data are from *Sherrod and Smith* [1989].

Area of Low to Zero Near Surface Heat Flow

Available drill-hole data are insufficient to define the area of low-to-zero near-surface conductive heat flow directly. We have assumed that this area includes most of the area where 0-2-Ma rocks are exposed and those areas with 2-7-Ma rocks where temperature profiles indicate nearly isothermal conditions (Figure 6a). Within the broad area of low-to-zero near-surface heat flow, there may be local near-surface heat flow highs due to

lower permeability, favorable topographic configuration, and (or) hydrothermal circulation. Site 87 (Figures 6 and 7) is an example of such a local hydrothermal disturbance. The thickness of the zone of low-to-zero conductive heat flow is poorly known and presumably highly variable. It may generally range from 150 to 1000 m thick. In the study area, only two drill holes collared in Quaternary rocks are deep enough to measure conductive heat flow beneath the nearly isothermal zone

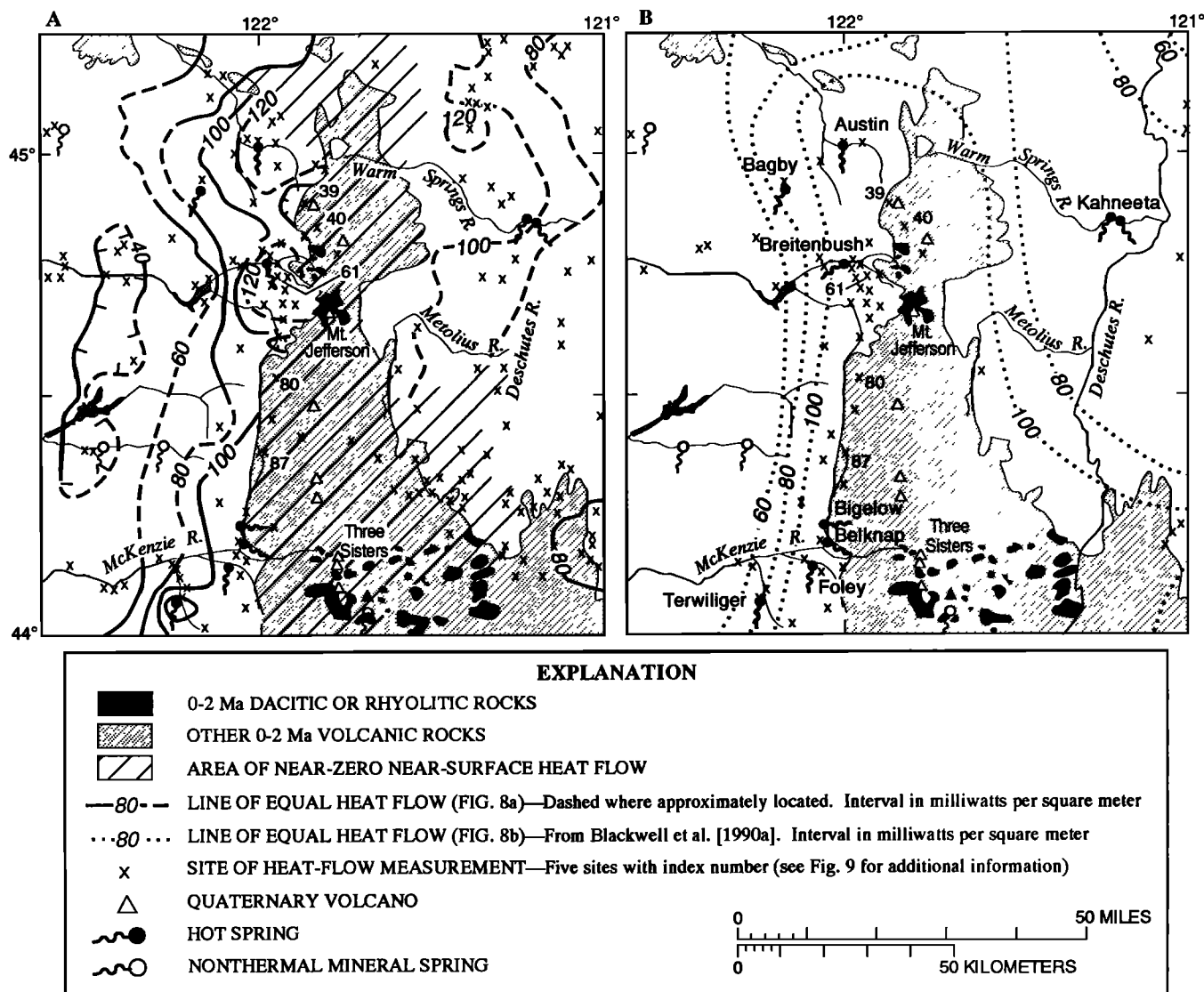


Fig. 6. (a) Conductive heat flow contours from Ingebritsen et al. [1991]. (b) Conductive heat flow contours from Blackwell et al. [1990a].

(Figures 6 and 7, sites 40 and 80). The temperature log from heat flow site 40 (CTGH-1 of Blackwell and Baker [1988b]) is nearly isothermal to depths in excess of 200 m and shows a linear conductive gradient below 650 m depth; the temperature log from site 80 (EWEB-TM of Blackwell et al. [1982]) is nearly isothermal to depths greater than 150 m and shows a linear gradient below 240 m depth. Sites 40 and 80 are both in topographically low areas, and the nearly isothermal zone may be substantially thicker beneath topographic highs. Swanberg et al. [1988] describe two core holes on the flanks of Newberry volcano, Oregon, that are isothermal at mean annual air temperature to depths of 900-1000 m. The deepest water wells in the 2-7-Ma rocks of the High Lava Plains penetrate to ~250 m depth and are nearly isothermal [Ingebritsen et al., 1988, 1991].

Areas of High Conductive Heat Flow

The heat flow highs in the older rocks of the Austin and Breitenbush Hot Springs areas and in the McKenzie River drainage (Figure 6) are relatively well documented [Blackwell et al.,

1990a]. The density of conductive heat flow data is greatest in the Breitenbush area (Figure 6), where temperature profiles suggest that the high conductive heat flow measured in rocks older than 7 Ma is a relatively shallow phenomenon. Seventeen shallow drill holes (<500 m deep) had high gradients that generally correspond to heat flow greater than 110 mW m⁻². However, a similar gradient in the upper part of the deepest hole (Figure 7, site 61) changed abruptly below a zone of thermal fluid circulation at ~800 m depth. That such a change was observed in the deepest hole suggests that the gradients in the shallow holes are also controlled by groundwater flow.

The heat-budget analysis of Ingebritsen et al. [1989, 1991] showed that sufficient heat is removed advectively from rocks younger than 7 Ma to explain the anomalous heat discharge measured on the flanks of the Cascade Range, so that a laterally extensive midcrustal heat source is not required. However, the heat-budget analysis cannot disprove the midcrustal heat-source model because of uncertainty regarding the magnitude and distribution of lower-temperature advective heat discharge [Ingebritsen et al., 1991].

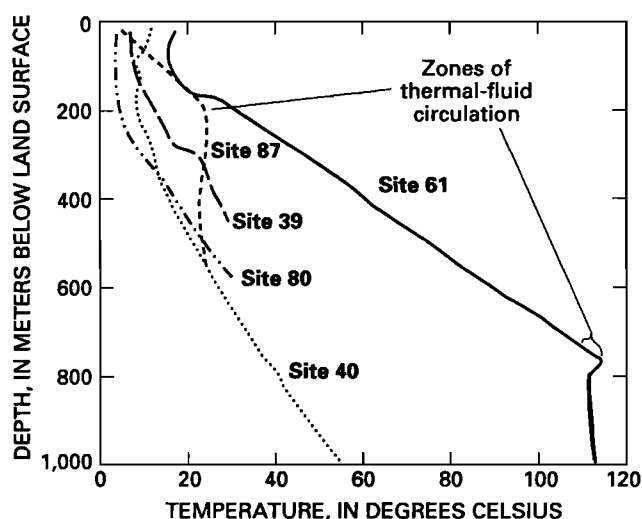


Fig. 7. Temperature-depth profiles from relatively deep drill holes (>460 m) in the study area. Our heat flow contours [Figure 6a] estimate conductive heat flow at depths of 100-200 m; when contouring the heat flow data, we ignored changes in gradient observed at greater depth in these holes. The deepest hole (site 61) was completed to 2457 m but was only logged to 1715 m. The bottom-hole (2457 m) temperature was at least 141 °C [Priest, 1985]. The gradient measured over the 1465 to 1715 m interval (31 °C km⁻²) projects to a bottom-hole temperature of 152 °C. See Figure 6 for site locations, and Ingebritsen et al. [1988, 1991] for additional information about each site. Sites 39, 80, and 87 are EWEB-SB, EWEB-TM, and EWEB-CL of Blackwell et al. [1982]; sites 40 and 61 are CTGH-1 and SUNEDCO 58-28 of Blackwell and Baker [1988b].

NUMERICAL SIMULATIONS

Numerical simulation can be used to examine some of the thermal and hydrologic implications of the alternate conceptual models depicted in Figure 2. We simulated groundwater flow and heat transport through two geologic cross sections west of the Cascade Range crest: one in the Breitenbush area, where there is no evidence for major arc-parallel down-to-the-east faulting, and one in the McKenzie River drainage, where major graben-bounding faults exist. The results provide some constraints on the regional permeability structure and also show that either model for the deep thermal structure can satisfy the near-surface heat flow observations.

The numerical code used for the simulations, PT [Bodvarsson, 1982], employs an integrated-finite-difference method to solve coupled equations of heat and energy transport that can be written

$$\int_V \frac{\partial}{\partial t}(\phi \rho) dV = - \int_A \rho v_d \cdot n dA + \int_V G_f dV \tag{3}$$

and

$$\int_V \frac{\partial}{\partial t}(\rho_m e) dV = - \int_A \lambda \nabla T \cdot n dA - \int_A \rho c_f \delta T v_d \cdot n dA + \int_V G_h dV \tag{4}$$

respectively, where *t* is time, ϕ is effective porosity, ρ and ρ_m are density of the fluid and the medium, respectively, *V* is volume, v_d is volumetric flow rate (Darcy velocity), *n* is a unit vector normal to a volume interface, *A* is area, *e* is internal energy of the medium, λ is medium thermal conductivity, *T* is temperature and δT denotes a volume-interface temperature, c_f is the

heat capacity of the fluid, and G_f and G_d are mass and heat source/sink terms, respectively. The volumetric flow rate (v_d) is calculated using Darcy's law. The mass and energy balance equations are coupled through pressure- and temperature-dependent parameters, as well as the source/sink terms.

The land surface defines the upper boundary of each cross section. We assumed that the water table is coincident with the land surface. This may be a poor approximation in some mountainous areas [see Forster and Smith, 1988], but in our particular cases the presence of abundant perennial streams and springs, generally shallow static water levels in wells [Ingebritsen et al., 1988, 1991], and high rates of groundwater recharge (Table 1) combine to suggest a relatively shallow water table. Simulated land-surface temperatures (12.8 °C - 5.5 °C per km above sea level) were based on the observed relation between spring temperature and elevation [Ingebritsen et al., 1991].

For each cross section we present selected steady state results that were obtained through long-term transient simulations. Initial conditions were a hydrostatic pressure distribution and temperature gradients of 50 °C km⁻¹ in the Quaternary arc and 30 °C km⁻¹ in the Western Cascades. The systems approached a steady state over simulation times of 10⁵ years or more. At simulation times of 10⁵ years, maximum rates of temperature change were typically less than 0.5 °C per thousand years. At simulation times of 10⁶ years, rates of temperature change were less than 0.02 °C per thousand years.

Table 3 describes lithologic units and the values of permeability, porosity, and thermal conductivity assigned to them. The values of porosity and thermal conductivity were used for all simulations, but permeabilities were varied about the listed values. Porosity is assumed to be inversely correlated with the age of the rock, and thermal-conductivity values are based on the data summarized by Ingebritsen et al. [1988, 1991].

Permeability Structure

Few permeability data are available for the study area, but two lines of evidence indicate that the older rocks are generally less permeable than the younger rocks. As discussed previously, groundwater recharge estimates show a rough inverse correlation between recharge rates and bedrock age (Table 1). Also, most 100- to 200-m-deep wells in rocks younger than about 7 Ma show pervasive advective disturbance, whereas 100- to 200-m-deep wells in older rocks have dominantly conductive temperature profiles. We can assume on this basis that the bulk permeability of the older rocks is relatively low, but the existence of hot springs and of localized advective disturbances (for example, Figure 7) in the older rocks are direct evidence for discrete zones of high permeability.

The older rocks lose primary permeability through hydrothermal alteration. Alteration of volcanic glass to clays and zeolites severely reduces permeability, as does recrystallization of glass to higher-temperature minerals. The extent of alteration depends largely on the primary permeability, glass content, and time-temperature history of the rock. We can roughly correlate loss of permeability with age because, in the study area, rocks of a certain age are lithologically similar and share a similar time-temperature history. The abundance of ash-rich sequences such as the Breitenbush Tuff in the 17-25 Ma age interval (Table 3, Tv₃) is an example of lithology influencing alteration patterns on a regional scale.

Keith [1988] noted that tuffaceous volcanic rocks affected by high-temperature (>200 °C) alteration consist mostly of anhy-

TABLE 3. Description of Rock Units and Values of Permeability, Porosity, and Thermal Conductivity Assigned in Numerical Simulations

Symbol Used on Cross Sections	Description	Permeability, m^2	Porosity	Thermal Conductivity, $W m^{-1} K^{-1}$
QTv	Chiefly lava flows and domes younger than 2.3 Ma	1.0×10^{-14}	0.15	1.55
Tv ₁	Lava flows and minor pyroclastic rocks from 4 to 8 Ma in age	5.0×10^{-16}	0.10	1.55
Tv ₂	Lava flows from 8 to 17 Ma in age (8-13 Ma in Breitenbush area)	1.0×10^{-16}	0.05	1.65
Tv ₃	Chiefly volcanic and volcanoclastic strata from 18 to 25 Ma in age (divided into Tv _{3u} and Tv _{3l} in Breitenbush area)	1.0×10^{-17} (Tv _{3u} : 5.0×10^{-17})	0.05	2.00 (Tv _{3u} : 1.50)
Tv _{3q}	Quartz-bearing ash-flow tuff in the Breitenbush area [Priest et al., 1987]	2.5×10^{-14}	0.02	2.00

drous minerals and are more easily fractured than rocks affected by lower-temperature alteration, so that secondary permeability may be relatively high. She suggested that a thermal aquifer in rocks affected by high-temperature alteration might consist of interconnected fractures at the same general stratigraphic horizon.

The simulations described herein place some limits on regional-scale permeabilities. Bulk permeabilities greater than about $10^{-17} m^2$ in the oldest rocks (Table 3, Tv₃) allow widespread advective heat transport; this is inconsistent with the heat flow data, which suggest that significant advective transport in these rocks is only very localized. Permeabilities less than about $10^{-14} m^2$ in the youngest rocks (QTv) lead to near-surface conductive heat flow values that are consistently higher than observed values from these rocks. For the intermediate-age units we assumed a rough inverse correlation between permeability and age.

A pronounced permeability-depth relation within each unit can also be inferred from the results of our simulations. Although the range of permeability values shown in Table 3 allows us to match the conductive heat flow observations, higher near-surface permeabilities are required to match the groundwater recharge estimates (Table 1). Well-test data from shallow (<50 m depth) domestic wells in the Western Cascades also indicate relatively high near-surface permeabilities, in the range of 10^{-14} - $10^{-12} m^2$ [McFarland, 1982].

Breitenbush Section

The 21.5-km-long Breitenbush cross section extends west-northwest from the Cascade Range crest through Breitenbush Hot Springs (Figures 8 and 9). Several 0.25-0.7 Ma dacite and rhyolite domes are found in the eastern part of the section (Figure 8), and the underlying silicic magmatic system is a possible heat source for the hydrothermal system [Smith and Shaw, 1975].

Temperature-depth data from the Breitenbush area define a broad area of elevated temperatures extending south of Breitenbush Hot Springs. The elevation of the 100-°C isotherm (Figure 8) is estimated from the elevation of the hot springs, temperature-depth data from heat flow site 61 (Figure 7), and projection

of terrain-corrected gradients from another 15 drill holes. The drill hole at site 61 (SUNEDCO 58-28 of Blackwell and Baker, 1988b) intercepted a thermal aquifer at ~800 m depth, in or near a quartz-bearing ash-flow tuff [Priest et al., 1987]. The spring orifices at Breitenbush Hot Springs are in the same stratigraphic unit [Priest et al., 1987], which suggests the presence of a stratigraphically controlled thermal aquifer, as does the broad upwarp in the 100-°C isotherm. We treated the quartz-bearing tuff as a 30-m-thick zone of relatively high permeability (Figure 9, unit Tv_{3q}). This unit is too thin to be shown as other than a heavy dashed line in Figure 9 and succeeding figures.

The hot springs lie within an electrically conductive zone identified from telluric data by H. Pierce and colleagues (written communication, 1989). These data suggest either two linear, electrically conductive structures (as shown in Figure 8) or curvilinear intertwined structures that splay and converge along a broadly northeast trend. In addition to the hot springs, the conductive zone encompasses two unusual low-discharge NaHCO₃ mineral springs. The 100-°C isotherm deepens abruptly northwest of the conductive zone (Figure 8). The conductive zone may represent fractures that channel thermal water to the surface or a relatively impermeable barrier that blocks lateral movement of thermal water.

A 6- to 7-km-deep integrated-finite-difference grid (Figure 9) was used to simulate groundwater flow and heat transport in the Breitenbush section; pressure and temperature solutions were calculated at 790 nodal points. The lateral boundaries were treated as no-flow (symmetry) boundaries; the lower boundary as a controlled-flux boundary (impermeable to fluid flow, with a specified conductive heat flow); and the upper (land surface) boundary as a constant pressure-temperature boundary (pressure of 1 bar, temperature varying with elevation). We simulated the thermal input for the alternate conceptual models depicted in Figure 2 by varying the conductive heat flow at the base of the cross section ("basal heat flow") and, in some cases, by introducing a shallow heat source beneath the Quaternary arc.

Figures 10 through 14 show selected steady state results from numerical simulations of the Breitenbush section. Simulated near-surface conductive heat flows were calculated using the temperature differences between the top two nodes in each column of nodes (Figure 9). The heat flow values thus represent

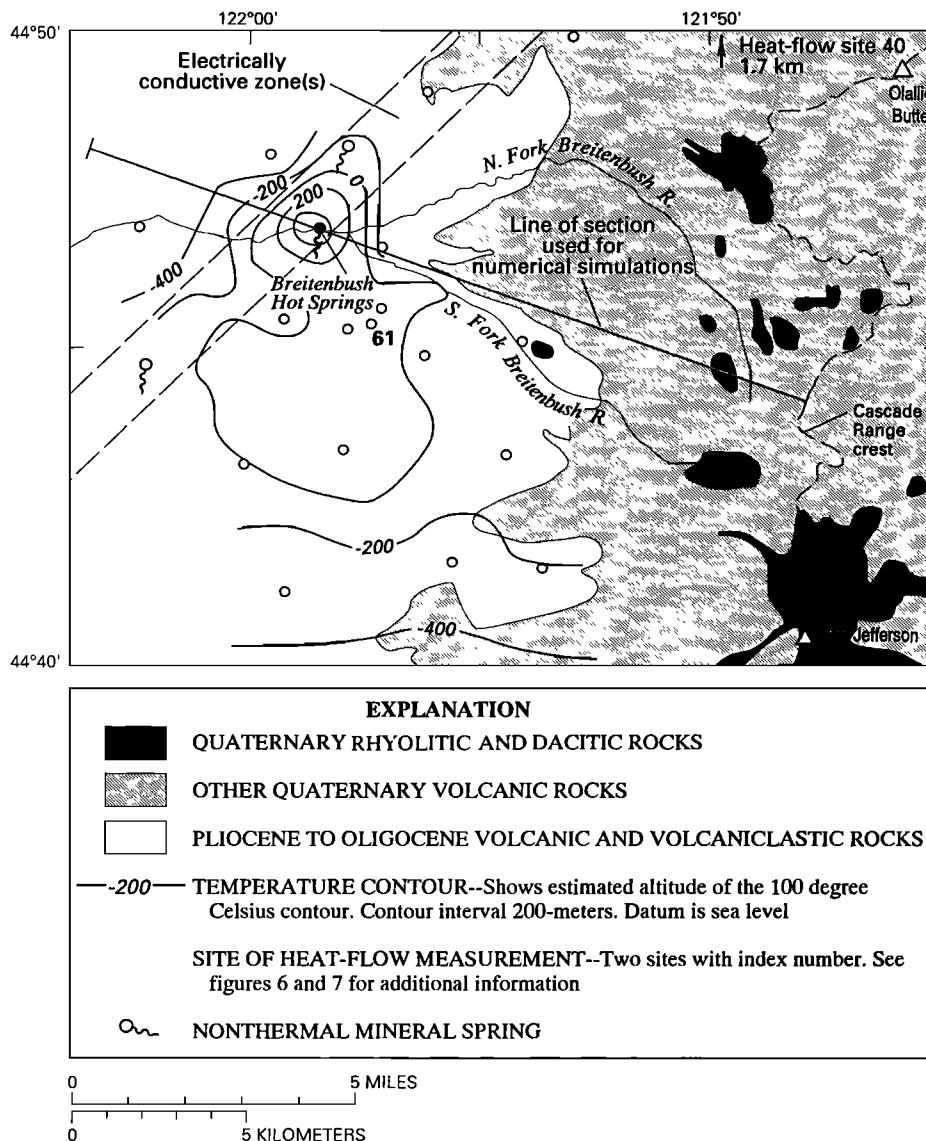


Fig. 8. Map of the Breitenbush Hot Springs area showing the line of section used in numerical simulations, the locations of thermal and nonthermal mineral springs, Quaternary volcanic rocks, the electrically conductive structures identified by H. Pierce et al. (written communication, 1989), and the estimated elevation of the 100 °C isotherm. Geologic data are from Priest et al. (1987) and from D.R. Sherrod and R.M. Conrey (unpublished data, 1988).

depths ranging from a few tens of meters to about 200 m, depths similar to those at which most of the conductive heat flow data were collected. The simulated recharge and discharge rates are the volumetric flow rates (Darcy velocities) between the top two nodes in each column. For convenience, both recharge (solid circles) and discharge (open circles) are plotted as positive quantities. The labeled arrows on Figure 10 and succeeding figures show how the heat supplied to and discharged from the system is partitioned between the Quaternary arc and the Western Cascades. These values ($J s^{-1}$) are calculated by assigning the two-dimensional section an arbitrary thickness of one kilometer. Because the Western Cascades comprise about two-thirds of the section, the total basal heat supplied to the Western Cascades is relatively large despite the lower basal heat flow.

The simulated results are compared with near-surface heat flow data projected onto the line of section, with groundwater recharge estimates (Table 1), and with temperature profiles from the deep (>1 km) drill holes at heat flow sites 40 and 61. Re-

sults from a conduction-only simulation with uniform basal heat flow (Figure 10a) were used to correct for topographic distortion of simulated heat flow values. In this simulation the minor transfer of heat ($0.61 \times 10^5 J s^{-1}$) from the Quaternary arc to the Western Cascades owes to topography and the relatively low thermal conductivity of the wedge of younger rocks.

Conduction-only simulations with narrow (Figure 10b) or wide (Figure 10c) basal heat flow anomalies failed to reproduce either the low near-surface conductive heat flow in the Quaternary arc or the elevated heat flow between Breitenbush Hot Springs and the Quaternary arc; some permeability is required. A simulation using a narrow heat flow anomaly and incorporating the permeability values listed in Table 3 (Figure 10d) provided a better match to the observed heat flow values, although simulated heat flow values between Breitenbush Hot Springs and the Quaternary arc are still mostly below the range of observed values.

In the simulation summarized in Figure 10d, most of the

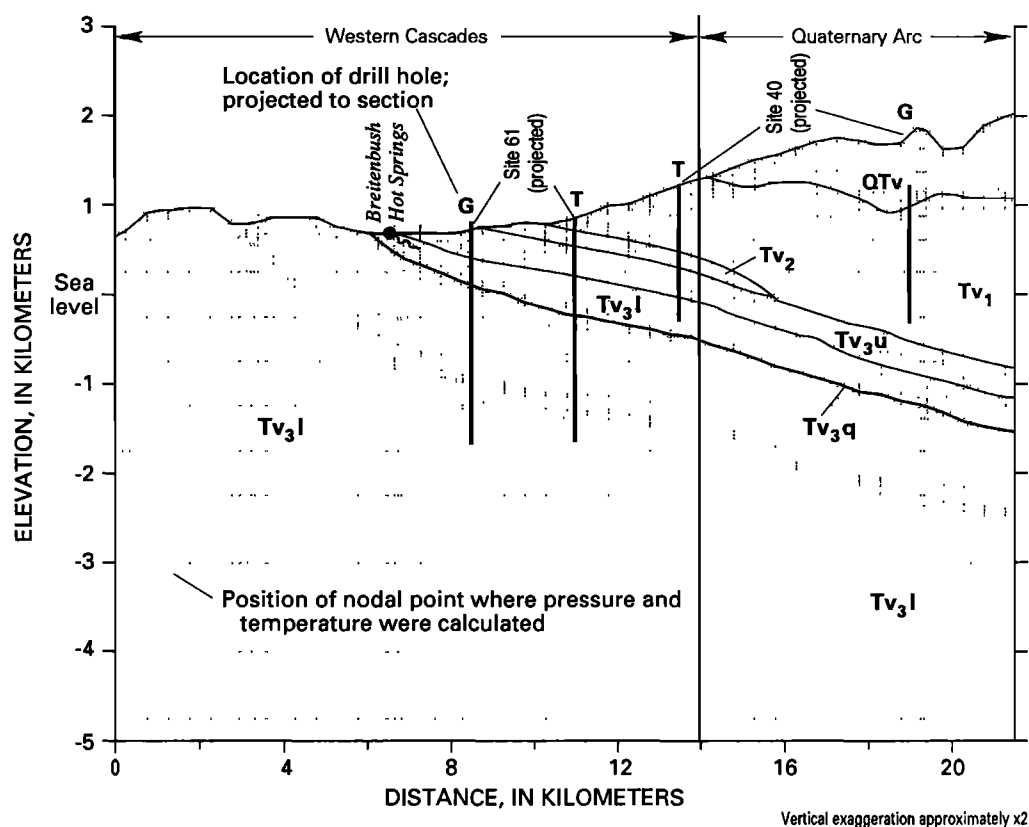


Fig. 9. Cross section used for numerical simulation of the Breitenbush Hot Springs system. Lithologic units are described in Table 3. Heat flow sites 40 (CTGH-1) and 61 (SUNEDCO 58-28), which lie off the section (Figure 8), are projected to the section in two different ways to indicate their appropriate geologic and topographic contexts. Geologic projection (G) locates the drill hole relative to stratigraphic contacts, and topographic projection (T) puts the collar elevation at the land surface.

groundwater recharged in the Quaternary arc (303 kg s^{-1}) discharges locally in topographic lows (301 kg s^{-1}) but carries little heat. Simulated discharge in the Breitenbush Hot Springs area ($\sim 1 \text{ kg s}^{-1}$) is a small fraction of total recharge in the Quaternary arc, but this relatively small mass flux transports substantial amounts of heat from the Quaternary arc to the Western Cascades. In this particular simulation the ratio of hot-spring discharge to recharge in the Quaternary arc (0.003) is similar to the ratio (0.002) that we estimated from measured groundwater recharge (Table 1) and hot-spring discharge rates (Table 2).

The simulated results are highly sensitive to permeability (Figures 11 and 12). Isotropic permeabilities 10 times lower than those listed in Table 3 (Figure 11a) led to near-surface heat flow values in the Western Cascades that are not significantly different from the conduction-only case of Figure 10b. Increasing permeability by ten-fold (Figure 11b) more closely matches the groundwater recharge estimates, but decreases heat flow between Breitenbush Hot Springs and the Quaternary arc to values well below those observed. Figures 11c and 11d illustrate the effects of moderate hydraulic anisotropy within each lithologic unit. In the simulation summarized in Figure 11c, horizontal permeabilities (k_x) are those listed in Table 3, whereas vertical permeabilities (k_y) are reduced by a factor of 10. In Figure 11d, k_y is 10 times higher than the k_x values listed in Table 3. Enhanced horizontal permeability might be explained by the layering of volcanic units; enhanced vertical permeability might be explained by pervasive vertical fractures. Evidence from New Zealand geothermal fields in volcanic rocks suggests $k_x/k_y \sim 10$

(P.R.L. Browne, oral communication, 1990), the case represented in Figure 11c.

The heat flow observations are best matched with the permeability values of Table 3 (Figure 10d). However, for the full range of permeability values illustrated (Figures 10d and 11), simulated hydrologic fluxes at the land surface are generally less than the minimum groundwater recharge calculated for rocks of similar ages (Table 1). Permeabilities higher than those of Figure 11b would be required to match the recharge estimates and would clearly cause excessive cooling. To match both the heat flow observations and the recharge estimates would require a strong permeability-depth relation within each unit, with near-surface (<50-m depth) permeabilities significantly higher than those used in our simulations. As noted above, well-test data from domestic wells in the Western Cascades [McFarland, 1982] support the inference of much higher permeabilities at relatively shallow depths.

The limited sensitivity analysis discussed above provides some constraints on the regional permeability structure but does not constrain the permeability of the thermal aquifer (unit Tv_3q), which was treated as a 30-m-thick zone of relatively high permeability. Figure 12 shows some effects of varying the permeability of unit Tv_3q independently within the overall permeability structures of Figures 10d (Table 3: $k = 1.0x$), 11a ($k = 0.1x$) and 11b ($k = 10x$). The results are summarized in terms of flow rates and temperatures in unit Tv_3q at the edge of the Quaternary arc. If the other units are assigned permeability values from Table 3 ($k = 1.0x$), assigning permeabilities less than about 10^{-14}

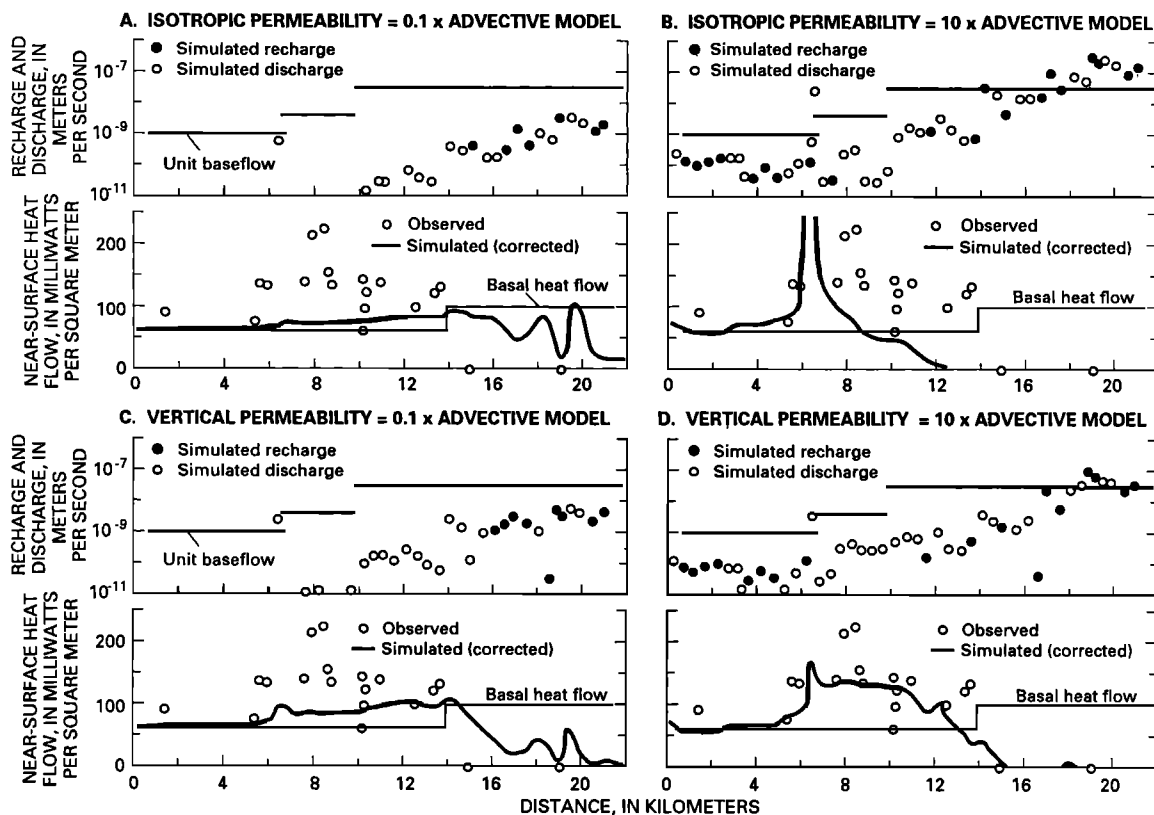


Fig. 11. Selected steady state results from numerical simulation of the Breitenbush section, showing sensitivity to permeability. Simulated heat flow values are compared with measured values, and simulated recharge and discharge rates are compared with the minimum recharge rates estimated for rocks of similar ages.

m^2 to Tv_3q restricts the volumetric flow rate and thus limits advective heat transfer. Assigning permeabilities greater than about $10^{-14} m^2$ to unit Tv_3q leads to significant cooling and thus reduces conductive heat flow between Breitenbush Hot Springs and the Quaternary arc. Permeabilities on the order of $10^{-14} m^2$ seem to be required for unit Tv_3q to function as an effective thermal aquifer, given its assumed thickness and the constraints on permeabilities of other units.

Although the simulation involving a narrow basal heat flow anomaly and the permeability values listed in Table 3 reproduced the near-surface heat flow values reasonably well, the temperature-depth profiles from the deep drill holes at heat flow sites 40 and 61 were matched poorly. A conduction-dominated simulation with a wide heat source and fluid flow confined to rocks younger than -2.3 Ma (Table 3, unit QTv) matched the data from site 40 fairly well, but failed to reproduce the high heat flow observed between Breitenbush Hot Springs and the Quaternary arc or the elevated gradient at site 61 (Figure 13). When fluid flow is confined to unit QTv , most heat supplied to the Quaternary arc discharges advectively there.

Figure 14 shows that both the near-surface heat flow data and the temperature-depth profiles from sites 40 and 61 can be reproduced reasonably well using two very different deep thermal structures, again with the permeability values listed in Table 3. The simulation summarized in Figure 14a involved uniform basal heat flow of $60 mW m^{-2}$ and an intense local heat source beneath the Quaternary arc, a situation analogous to the lateral-flow model (Figure 2a); the simulation in Figure 14b involved a wide basal heat flow anomaly of $130 mW m^{-2}$, analogous to the

midcrustal heat source (Figure 2b). The total heat supplied to the system in these two simulations is identical. Both simulations match the observations reasonably well. In these simulations (Figure 14), the rates of advective heat transfer from the Quaternary arc to the Western Cascades (0.7 - 1.2 MW) are similar to the length-normalized rate of heat transfer by the hot-spring systems ($121 MW \div 135 km$ arc length = $0.9 MW/km$ arc length; see Figure 5 for measured values).

Our simulations cannot simultaneously match the temperature profile from site 61 and the near-surface heat flow data. If the simulated temperature at the depth of the thermal aquifer (~ 800 m) matched the measured temperature exactly, near-surface conductive heat flow between Breitenbush Hot Springs and the Quaternary arc would greatly exceed the observed values. (See, for example, Figure 14, where simulated heat flows are higher than most observed values despite thermal-aquifer temperatures that are lower than those observed.) This implies that the actual fluid-flow geometry is probably more complex than in the system we simulated. For example, the geometry of unit Tv_3q may be different, and focusing of flow in the third (unsimulated) dimension may be important. Three-dimensional effects certainly create some of the scatter in the observed heat flow data that are projected to the section, and the nonuniform distribution of hot-spring heat transport (Figure 5) indicates significant three-dimensional focusing of fluid flow.

Different ways of matching the temperature profile from heat flow site 61 carry distinct implications about the age of the hydrothermal system. Under nearly steady state conditions ($>10^5$ years), the low temperature gradient below 800 m depth is best

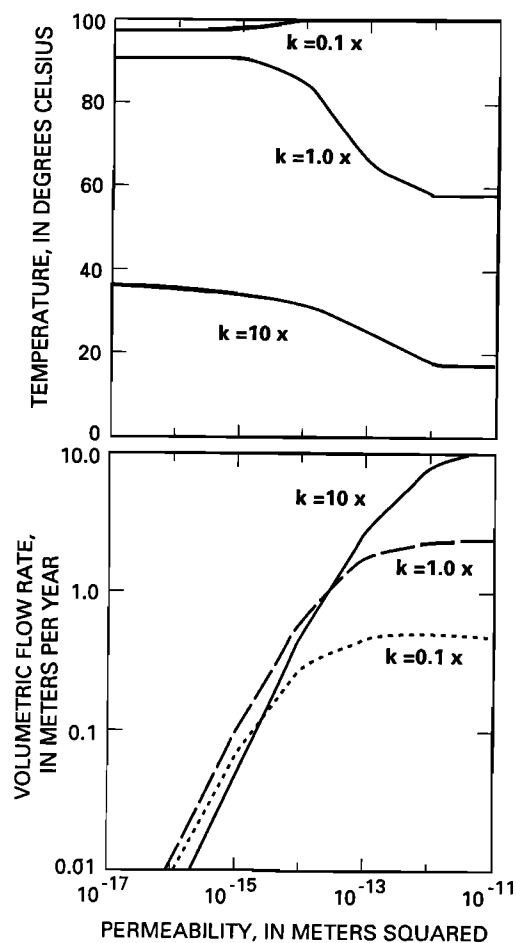


Fig. 12. Relation between the permeability of unit Tv_3q and temperature and volumetric flow rate (Darcy velocity) in Tv_3q at the edge of the Quaternary arc. Overall permeability structures are those of Figures 10d ($k = 1.0x$), 11a ($k = 0.1x$), and 11b ($k = 10x$).

matched with a relatively low basal heat flow. The temperature gradient measured across the 1465-1715-m depth interval was $31\text{ }^{\circ}\text{C km}^{-1}$ and predicts a bottom-hole (2457 m) temperature of $152\text{ }^{\circ}\text{C}$, which is consistent with the measured bottom-hole temperature of at least $141\text{ }^{\circ}\text{C}$ [Priest, 1985]. This gradient corresponds to a heat flow of $\sim 68\text{ mW m}^{-1}$ [Ingebritsen et al., 1988, 1991]. If flow in the thermal aquifer has been relatively short lived ($\sim 10^4$ years), the observed profile can be closely matched with a much higher basal heat flow. For example, Blackwell and Baker [1988a; Blackwell et al., 1990a] used a heat flow of 124 mW m^{-2} and a time of 2.5×10^4 years to obtain a good match. If the hydrothermal system is driven by a long-lived silicic magmatic system such as fed the 0.25-0.7-Ma dacite domes in the eastern part of the cross section, the near-steady state match is more appropriate. In either case, volumetric flow rates (Darcy velocities) on the order of 1 m yr^{-1} are required to maintain elevated aquifer temperatures.

In conclusion, regardless of the conceptual model invoked for the deep thermal structure, significant advective heat transport is required to reproduce several of the observations from the Breitenbush area, including the near-zero near-surface heat flow in the Quaternary arc, elevated heat flow between Breitenbush Hot Springs and the Quaternary arc, and the major decrease in the temperature gradient below ~ 800 m depth at heat flow site 61. Advective heat transport precludes the half-width

modeling invoked by Blackwell et al. [1990b]. The deep thermal structure cannot be uniquely inferred from the available temperature-depth observations.

McKenzie River Section

The 44-km-long McKenzie River cross section extends west from the Cascade Range crest through Terwilliger Hot Spring (Figure 15). Silicic volcanic rocks exposed near the eastern end of the section in the South Sister area (Figure 15) include Pleistocene and Holocene rhyolite and dacite; thus the underlying silicic magmatic systems may drive hydrothermal activity.

Temperature-depth data are sparser in the McKenzie River area than in the Breitenbush area, and deep (>1 km) drill-hole data are lacking. In the McKenzie River cross section we have experimented with hypothetical 30-m-thick stratigraphically controlled aquifers at three different depths (Figure 16), although there is no direct evidence for such aquifers.

The four hot springs in the McKenzie River drainage (Figure 15) are located near arc-parallel faults or fracture zones that likely interrupt the flow of groundwater down the hydraulic gradient from the Quaternary arc [Priest et al., 1988]. Three of the four are close to and probably associated with the Horse Creek fault zone; the fourth and westernmost is near the Cougar Reservoir fault zone. Cumulative mapped offset on the Horse Creek fault zone is as much as 850 m south of the McKenzie River; offset on the Cougar Reservoir fault zone may be comparable [Priest et al., 1988].

Relatively chloride-rich waters sampled at several localities away from the hot springs suggest a "leaky" thermal system in the area. Dilute Na-Cl water from a 62-m-deep well at White Branch Youth Camp could contain approximately 5% thermal water, and the Bigelow thermal well discharges thermal water compositionally similar to that from Belknap Springs (see Figure 15 for well locations). The unnamed spring between Foley Springs and White Branch Youth Camp (Figure 15) is anomalously high in chloride, as are Separation Creek and the White Branch of McKenzie River [Ingebritsen et al., 1988, 1991]. The anomalous chloride flux in Separation Creek ($\sim 10\text{ g s}^{-1}$) is larger than the fluxes from some of the hot springs in the study area (Table 2). This widespread evidence for diffuse discharge of thermal water is consistent with data from the U.S. Geological Survey stream-gaging station near Vida (Figure 15), which suggest that the total discharge of high-chloride water is somewhat greater than the sum of the individual hot springs [Mariner et al., 1990; Ingebritsen et al., 1991].

Pressure and temperature solutions for the McKenzie River section were calculated at 921 nodal points within a 5.5- to 7.5-km-deep integrated-finite-difference grid (Figure 16). The boundary conditions were the same as those used in simulations of the Breitenbush section: the lateral boundaries were no-flow boundaries, the lower boundary a controlled-flux boundary, and the upper boundary a constant pressure-temperature boundary. We again simulated the thermal input for the alternate thermal structures (Figure 2) by varying the distribution of deep heat sources. Except where otherwise noted, lithologic units and rock properties are those listed in Table 3.

We treated the faults (Figure 16) as 30-m-wide zones of relatively high vertical permeability. The presence of several fault zones and the major topographic divide between Horse Creek and Cougar Reservoir make the McKenzie River section significantly different from the Breitenbush section; the degree of

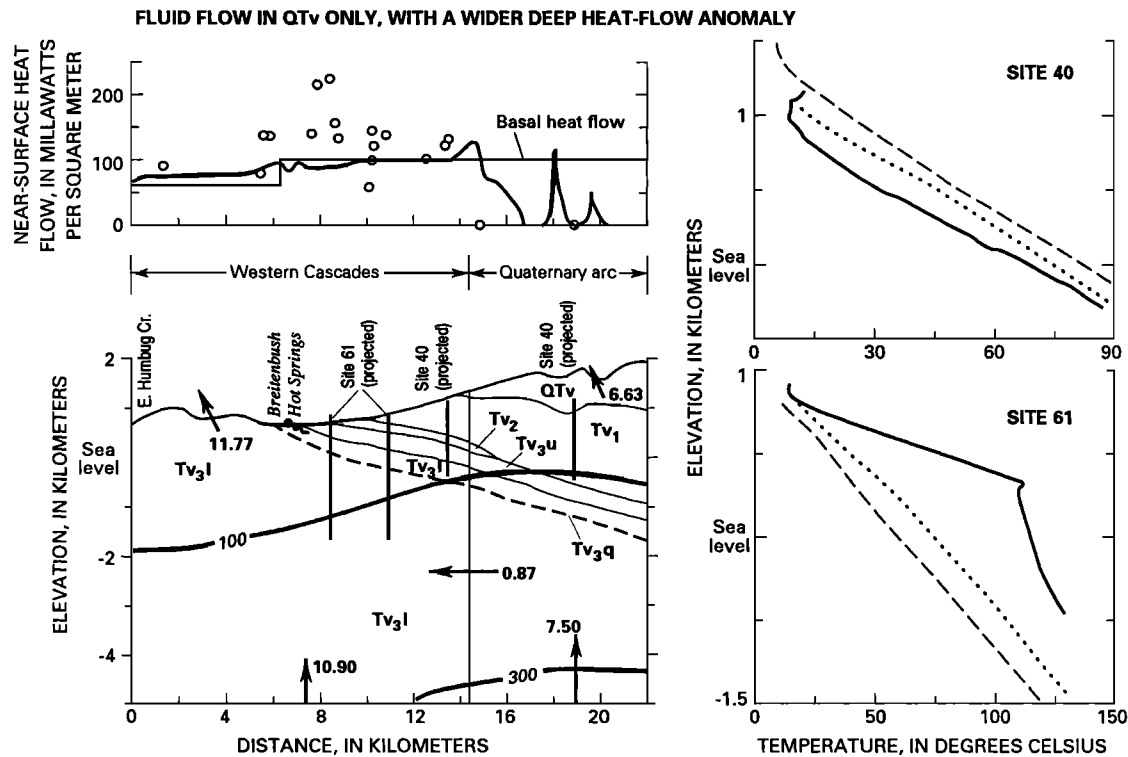


Fig. 13. Results from a simulation involving a wide basal heat flow anomaly and fluid flow only in unit QTv. This simulation fails to match the high heat flow between Breitenbush Hot Springs and the Quaternary arc or the elevated temperature gradient measured to depths of ~800 m at heat flow site 61. Because heat flow sites 40 and 61 are off section (Figure 8), we compare the data from each hole with two simulated temperature profiles. One projection ("geologic") puts the hole in stratigraphic context, the other ("topographic") places the collar elevation at the land surface.

continuity of regional groundwater flow across these barriers is one of the major issues of interest.

Figures 17, 18, and 19 show selected results from numerical simulations of the McKenzie River section. Simulated near-surface heat flow values are compared with data projected onto the line of section, and volumetric flow rates (Darcy velocities) in the hypothetical aquifer units are shown for some cases. Results from a conduction-only simulation with uniform basal heat flow (Figure 17a) were used to correct for topographic distortion of simulated heat flow values.

As was the case with the Breitenbush section, conduction-only simulations with narrow (Figure 17b) or wider (Figure 17c) basal heat flow anomalies failed to reproduce the near-surface heat flow observations. However, the heat flow data are concentrated near the Horse Creek and Cougar Reservoir fault zones (Figure 15). The elevated heat flow in those areas (Figure 17) could be explained in terms of convective (density-driven) circulation within the fault zones themselves, with insignificant advective heat transport in the two dimensions that we simulated, although such relatively local circulation would be inconsistent with some of the geochemical evidence discussed above.

Figure 17d summarizes the results of three simulations in which aquifer depth was varied. The 30-m-wide fault zones and the aquifer were assigned permeabilities of $2.5 \times 10^{-14} \text{ m}^2$. These simulations resulted in pronounced conductive heat flow anomalies at the Horse Creek and Cougar Reservoir fault zones and in the Separation Creek area but resulted in very low heat flow between the two fault zones. In each of these simulations, advective heat transfer between the Quaternary arc and the

Western Cascades is small, amounting to less than 10% of the heat supplied to the Quaternary arc; most of the heat supplied to the Quaternary arc discharges in the Separation Creek area or at the Horse Creek fault zone. Only for the deepest aquifer configuration is there continuous regional groundwater flow and a net transfer of heat from the Quaternary arc to the Western Cascades (see the volumetric flow rates and labeled arrows in Figure 17d). For the shallower aquifer configurations there is actually net heat transfer from the Western Cascades to the Quaternary arc, because some groundwater recharged in the Western Cascades discharges in the Horse Creek area.

Simulated heat transfer between the Quaternary arc and the Western Cascades is sensitive to the permeability structure. Net heat transfer is increased by reducing the permeability of the upper (dashed) part of the Horse Creek fault zone to values similar to those assigned to the rocks surrounding the fault zone (Figure 18a); incorporating 30-m-wide high-permeability (2.5×10^{-14}) conduits (dikes, Figure 16) for deep recharge within the Quaternary arc (Figure 18b); and lowering the permeability of the 8-17-Ma lava flows (Table 3, Tv_2) to $2 \times 10^{-17} \text{ m}^2$ (Figure 18c). If these relatively minor modifications to the poorly constrained permeability structure are combined (Figure 18d), the net heat transfer is significant, and near-surface conductive heat flow between the Horse Creek and Cougar Reservoir fault zones is greater than the basal heat flow in that area.

Reduced permeability in the upper part of the Horse Creek fault zone (Figure 18a) might be explained by hydrothermal alteration and (or) silica deposition. Note that if the permeabilities of the Horse Creek and Cougar Reservoir fault zones are

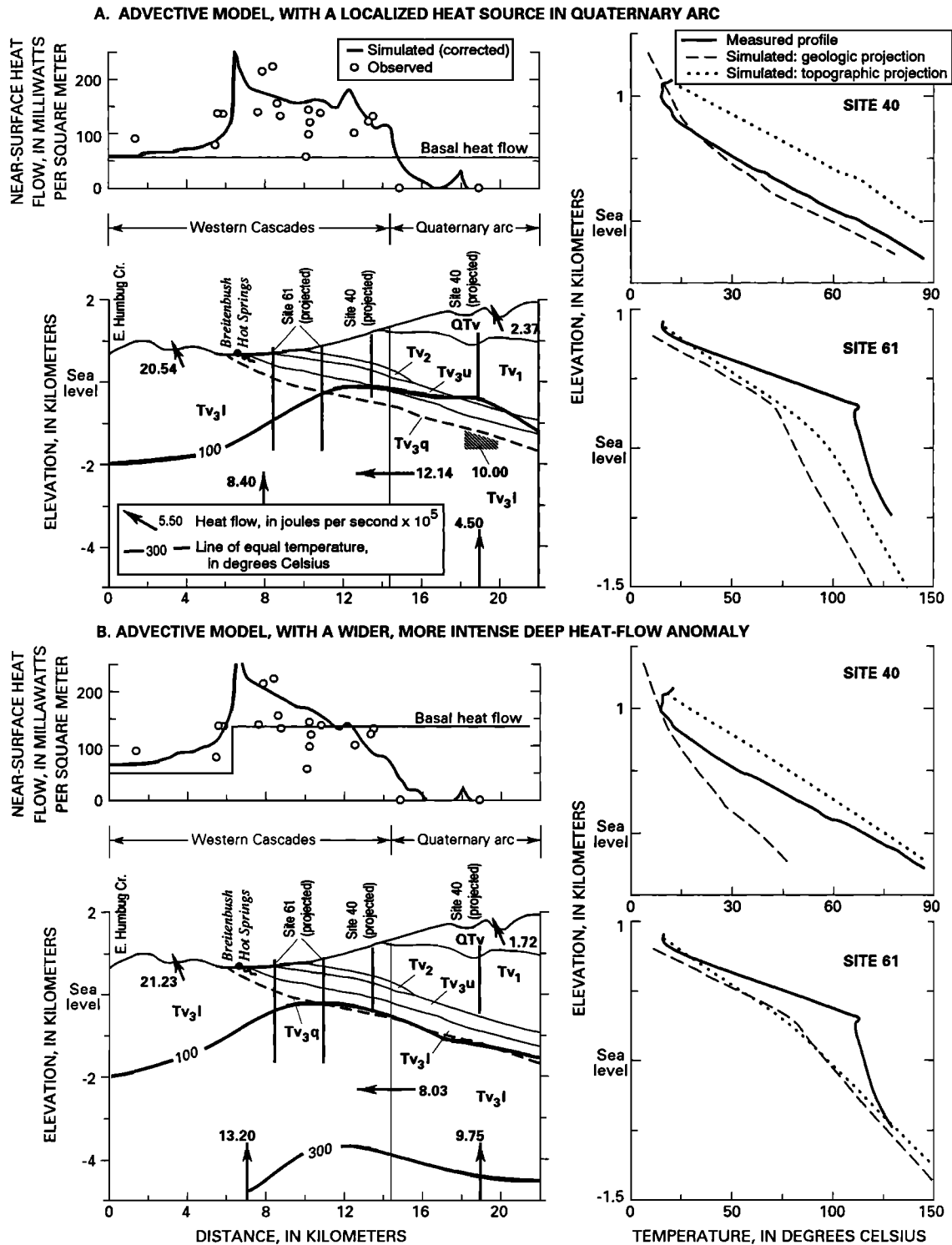


Fig. 14. Selected results from numerical simulation of the Breitenbush section, showing that the thermal observations can be reproduced reasonably well with two very different deep thermal structures. In Figure 14a, the dark polygon in unit Tv₃l indicates the location of a heat source (an upper-crustal magma body) producing $10.0 \times 10^5 \text{ J s}^{-1}$. See captions to Figures 9 and 13 for explanation of geologic and topographic projections of heat flow sites 40 and 61.

equal (for example, Figure 17d), heated groundwater is discharged preferentially at Horse Creek, with relatively minor hydrothermal effects at Cougar Reservoir. Over time, focused discharge at Horse Creek could lead to decreased permeability. Silica deposition might be concentrated in the upper part of the fault zone, where temperature gradients are relatively steep.

As with the Breitenbush section, very different distributions of deep heat sources can produce similar matches to the available data. However, unlike the Breitenbush case, one of the matches that we consider reasonable for the McKenzie River section is conduction dominated. A conduction-dominated simulation with a wide basal heat flow anomaly and fluid flow

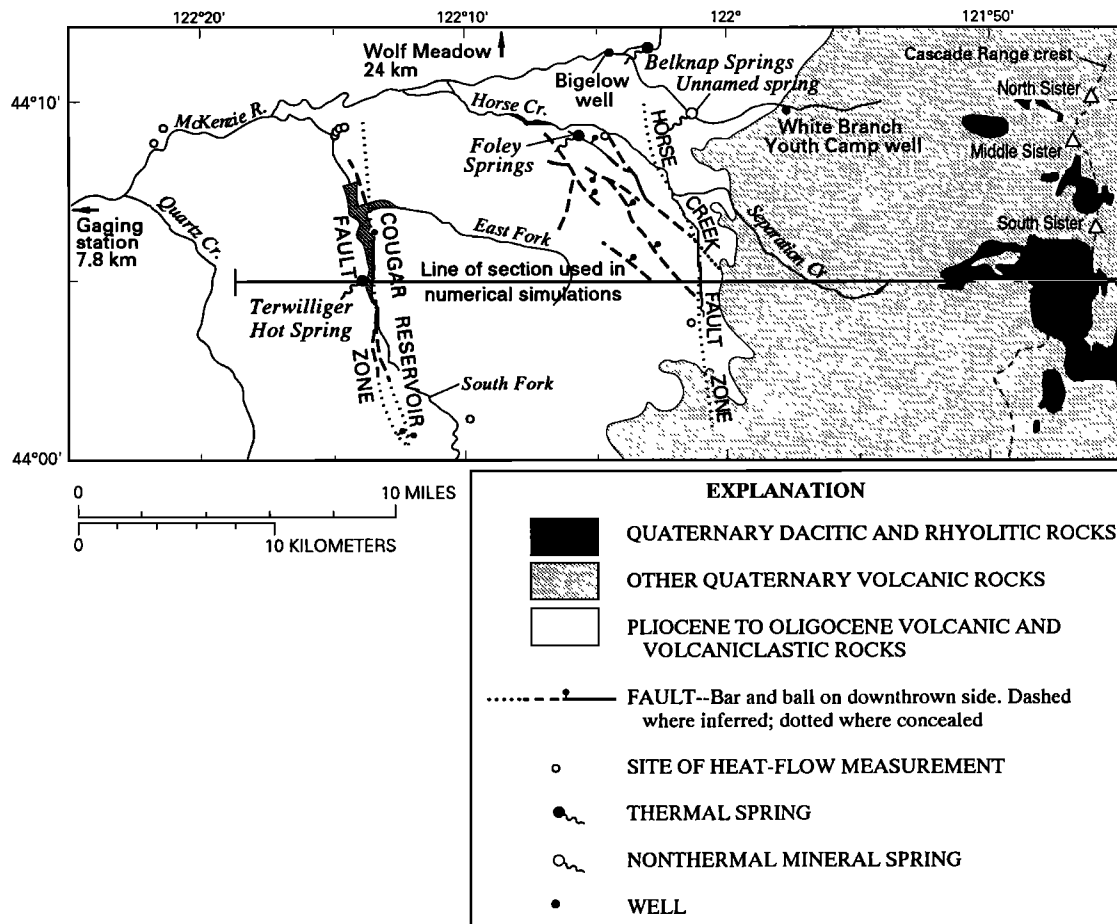


Fig. 15. Map of the McKenzie River area showing the line of section used in numerical simulations, the locations of thermal springs and other springs and wells discussed in the text, faults, and Quaternary volcanic rocks. Geologic data are from Priest *et al.* [1988] and from our own unpublished compilation map.

confined to unit QTv (Figure 19a) is analogous to the midcrustal heat source model (Figure 2b) and provides a reasonable match to the available data; elevated heat flow near the Horse Creek and Cougar Reservoir fault zones can be explained in terms of convection in a third (unsimulated) dimension, as noted above. Simulations involving localized heat sources, which are analogous to the lateral-flow model (Figure 2a), can also match the thermal data (for example, Figure 19b); they involve advective heat-transfer rates (0.9-1.8 MW) that are roughly comparable to the measured rates of heat transfer by hot-spring systems (0.9 MW/km arc length).

In conclusion, the shallow, sparser thermal observations in the McKenzie River area allow conduction- or advection-dominated numerical simulations. Advection-dominated models lead to elevated heat flow in the highlands between the Horse Creek and Cougar Reservoir fault zones only if there is a thermal aquifer at depths of several kilometers. At shallower depths, regional groundwater flow may be interrupted by the Horse Creek fault zone and the topographic divide between the fault zones. Blackwell *et al.* [1990a, p. 19,484] argue against the lateral-flow model (Figure 2a) on the basis of a high conductive gradient measured in the "Wolf Meadow hole", which is located north of the McKenzie River in a topographic position somewhat analogous to the highlands between Horse Creek and Cougar Reservoir (Figure 15). Our results show that regional

groundwater flow could influence heat flow measurements at similar high-elevation sites in the Western Cascades.

Heat Transfer Rates and Residence Times

Actual patterns of fluid circulation are certainly more complex than the representations in our two-dimensional sections. For example, topographic variations in the unsimulated (north-south) dimension presumably act to focus thermal-fluid discharge in the deeply incised valleys of the Western Cascades. Nevertheless, a comparison of simulated and measured heat-transfer rates is a useful test of the simulated results.

In advection-dominated simulations that match the observations reasonably well (Figures 14 and 19b), rates of advective heat transfer from the Quaternary arc to the Western Cascades range from 0.7 to 1.8 MW per kilometer of arc length. These values encompass the length-normalized measured value of 0.9 MW per km arc length. Our cross sections include hot-spring areas, and these simulated heat-transfer rates allow us to match observed conductive heat flow values that are considerably in excess of 100 mW m^{-2} . A lower rate of $\sim 0.5 \text{ MW per km arc length}$ would be sufficient to support conductive heat flow of $\sim 100 \text{ mW m}^{-2}$ between Breitenbush Hot Springs and the Quaternary arc (Figure 10d). Such relatively low advective heat-transfer rates might be typical of the areas between hot-spring

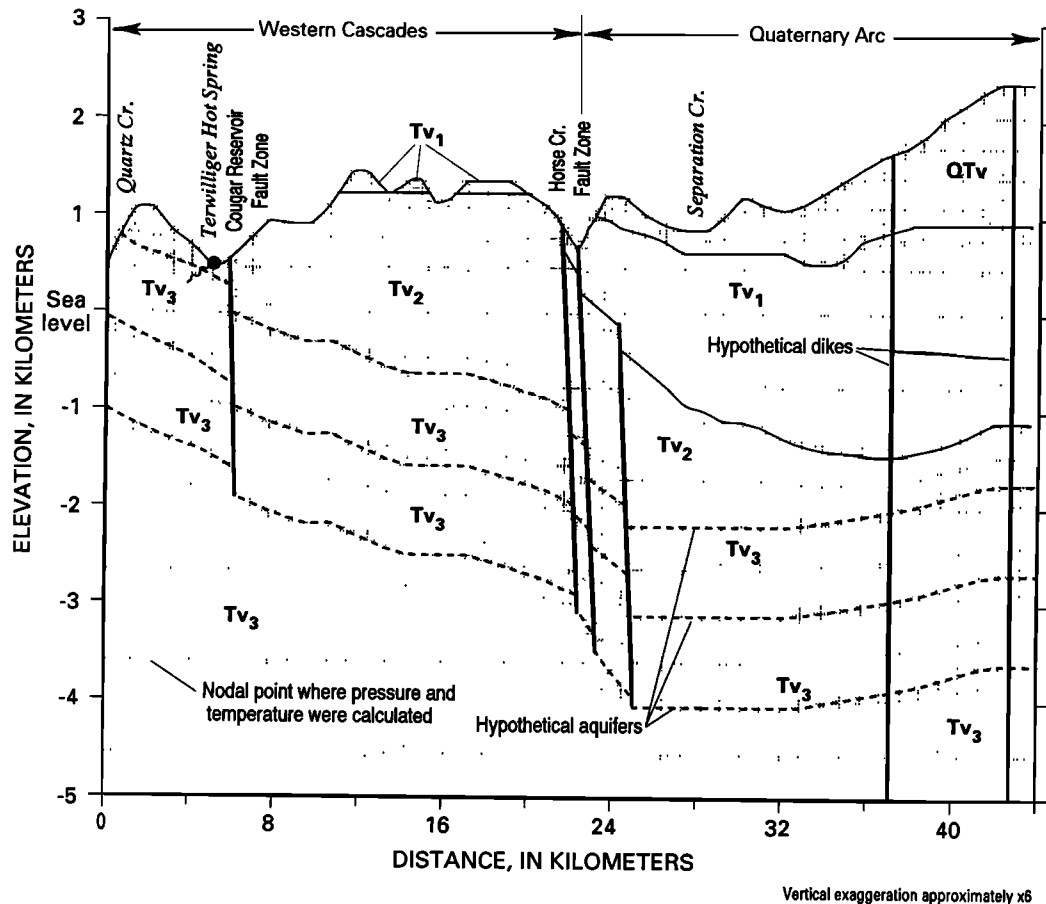


Fig. 16. Cross section used for numerical simulation of the McKenzie River area. Lithologic units are described in Table 3. The hypothetical dikes underlie silicic vents near South Sister; zones of relatively high vertical permeability associated with such dikes could enhance deep recharge in the Quaternary arc.

Thermal-fluid residence times are only weakly constrained by the available data. Sulfate-water isotopic equilibrium implies minimum residence times of 40 to 2000 years, and our interpretation of the stable-isotope data implies maximum residence times of less than 10,000 yr. Simulated volumetric flow rates (v_d) in the thermal aquifers are on the order of 1 m yr^{-1} (e.g., Figure 19b), and similar rates are required to maintain the elevated thermal-aquifer temperature observed at heat flow site 61 (Figure 7). Fluid particle velocities are approximated by v_d/ϕ , where ϕ is effective porosity. Thus for ϕ equal to 0.02 (Table 3), fluid velocities in the thermal aquifer are $\sim 50 \text{ m yr}^{-1}$, and thermal-aquifer residence times are a few hundred years. Rates of vertical recharge through the less permeable layers that confine the thermal aquifer are much lower, so that simulated particle velocities are as low as 0.1 m yr^{-1} , and total residence times exceed 10,000 years. The addition of localized conduits for deep recharge (Figures 18b, 18d, and 19b) reduces total residence times to less than 1000 years. If our interpretation of the stable-isotope data is correct, recharge to thermal aquifers must occur through discrete zones with relatively high vertical permeability. Such vertical conduits might be created by intrusions or by normal faulting.

REGIONAL GRAVITY, MAGNETIC, AND ELECTRICAL GEOPHYSICAL DATA

Regional geophysical data afford another possible means of discriminating the alternate models for the deep thermal struc-

ture (Figure 2). For example, midcrustal, regional-scale geothermal phenomena may be expressed in regional gravity data [e.g., Blackwell *et al.*, 1982, 1990a], and we have investigated this relation in the study area in some detail. Figure 20 shows the relation between gravity and heat flow values from the study area. For every heat flow datum, a corresponding gravity value was interpolated from a gridded representation of regional gravity. This approach allows us to examine the nature and strength of any correlation between gravity and heat flow, but it is limited by the nonuniform distribution of heat flow data (Figure 6).

West of the Cascade crest there is a weak negative correlation between Bouguer gravity and heat flow, with a "step" change in Bouguer gravity values associated with a heat flow of approximately 60 mW m^{-2} (Figure 20a). However, on a regional basis there is no correlation between wavelength-filtered residual gravity and heat flow (Figure 20b) or between isostatic residual gravity and heat flow (Figure 20c). Locally, a persistent negative correlation between gravity and heat flow in the vicinity of Mount Hood (Figures 20a-20c) can be largely explained as a relict of strong correlations between elevation and heat flow and elevation and gravity.

The wavelength-separated residual gravity was derived by spectral separation at a wavelength of approximately 90 km. Wavelength filtering at this threshold minimizes the effects of sources at depths greater than approximately 20 km [Couch *et al.*, 1982a], although it also will eliminate anomalies that result

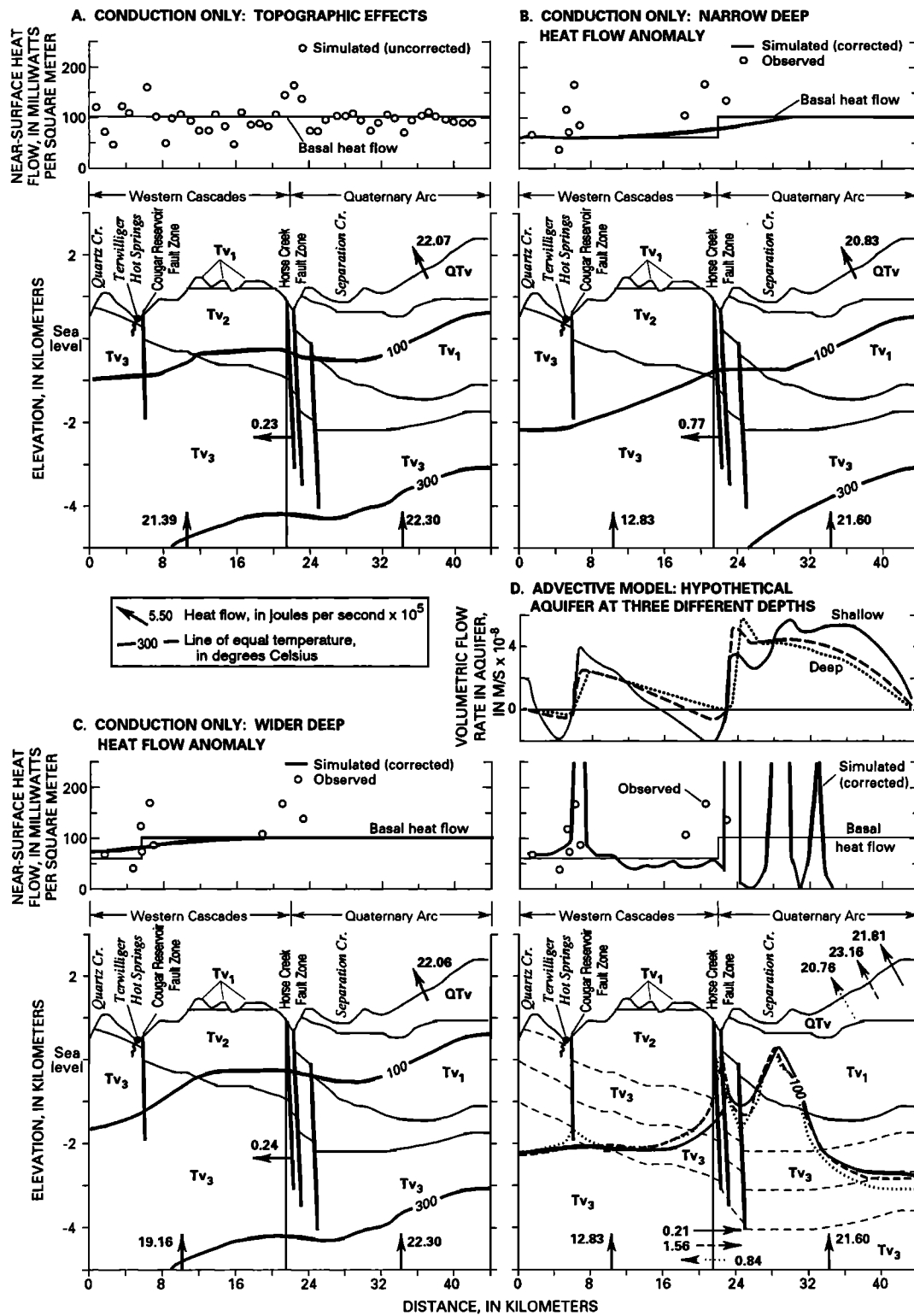


Fig. 17. Selected steady state results from numerical simulation of the McKenzie River section. The conduction-only case of Figure 17a was used to correct simulated near-surface conductive heat flows from other simulations. Simulated heat flow values are compared with measured values and, in Figure 17d, simulated volumetric flow rates (Darcy velocities) in the deep "aquifer" unit are shown. Labeled arrows indicate how the heat supplied to the system is partitioned. In Figure 17d, the solid, dashed, and dotted lines and arrows indicate results for the shallowest, intermediate, and deepest "aquifer" configurations, respectively.

from long-wavelength lateral density variations at shallow depth. The isostatic residual data have been processed to remove topographically induced regional trends and to enhance gravity anomalies related to crustal geologic features. These

data are produced using an Airy-Heiskanen model for isostatic compensation, by subtracting the calculated effect of a crust-mantle interface from the Bouguer values [Simpson *et al.*, 1986]. Any correlation between gravity and heat flow that is due to a

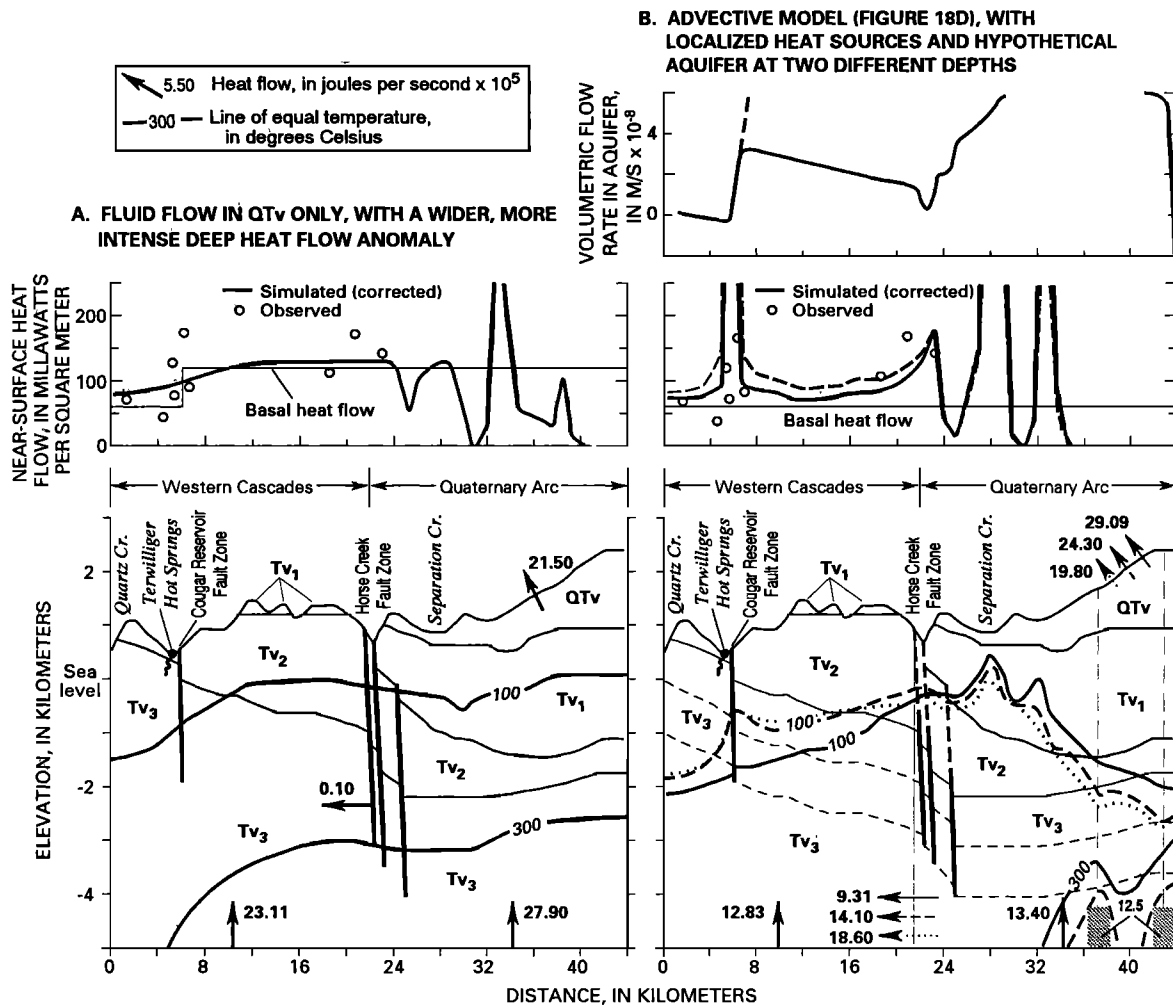


Fig. 19. Selected results from numerical simulation of the McKenzie River section, showing that the sparse near-surface heat flow observations can be matched with a conduction-dominated model involving fluid flow only in QT_v (Figure 19a) or an advection-dominated model with localized heat sources (Figure 19b). The total heat input to the system in these two simulations was identical. In Figure 19b, the solid and dashed lines and arrow indicate results for the shallower and deeper aquifer configurations, respectively. The dotted lines and arrow indicate results from a simulation in which both aquifers were present. The labeled dark rectangles in Figure 19b indicate localized heat sources each producing $12.5 \times 10^5 \text{ J s}^{-1}$; the permeability structure is that of Figure 18d.

than that between Bouguer gravity and heat flow (note the change in vertical scale between Figures 20a and 20d). However, the apparent relation has a similar form, with a "step" change in gravity at approximately 60 mW m^{-2} . The local negative correlation in the vicinity of Mount Hood, which persisted through the other forms of processing, is eliminated by upward continuation (Figure 20d). *Blakely and Jachens* [1990] applied a boundary-locating technique to upwardly continued isostatic residual gravity data from Washington, Oregon, and northern California. They identified a density boundary approximately 40 km west of the Three Sisters at 44° N latitude, and noted that it roughly coincides with the heat flow transition mapped by *Blackwell et al.* [1982]. *Blakely and Jachens* [1990] also noted that the density boundary might reflect a geologic contact associated with a fault postulated by *Sherrod* [1986, Figure 21], and not a thermal discontinuity.

Connard et al. [1983] and *Foote* [1985] analyzed aeromagnetic measurements from the Cascade Range in central and northern Oregon to determine the depth extent of magnetic sources. They interpreted the basal source depth to represent the

Curie-temperature isotherm, which is defined as the temperature at which rocks become essentially nonmagnetic. *Connard et al.* [1983] noted that Curie-point temperatures in the crust may range from 300 to 580 $^\circ\text{C}$.

Curie-depth estimates are susceptible to the problems of uniqueness inherent to all inverse methods, and the basal depth of magnetic sources may not represent an isothermal surface: both the Curie temperature and other rock magnetic properties may vary from place to place [*Blakely*, 1988]. Despite these uncertainties, a high degree of spatial correlation between shallow Curie depths and high near-surface heat flow would be persuasive evidence for the extensive midcrustal heat source model (Figure 2b). An area of shallow Curie depths that is more closely confined to the Quaternary arc would be consistent with the lateral-flow model (Figure 2a).

Figure 21 shows the relation between near-surface heat flow, Curie-depth estimates, and the area of Quaternary vents. The precise locations of the Curie-depth boundaries are uncertain because the spatial resolution of the Curie-depth estimates is relatively poor. *Connard et al.* [1983] resolved source depths

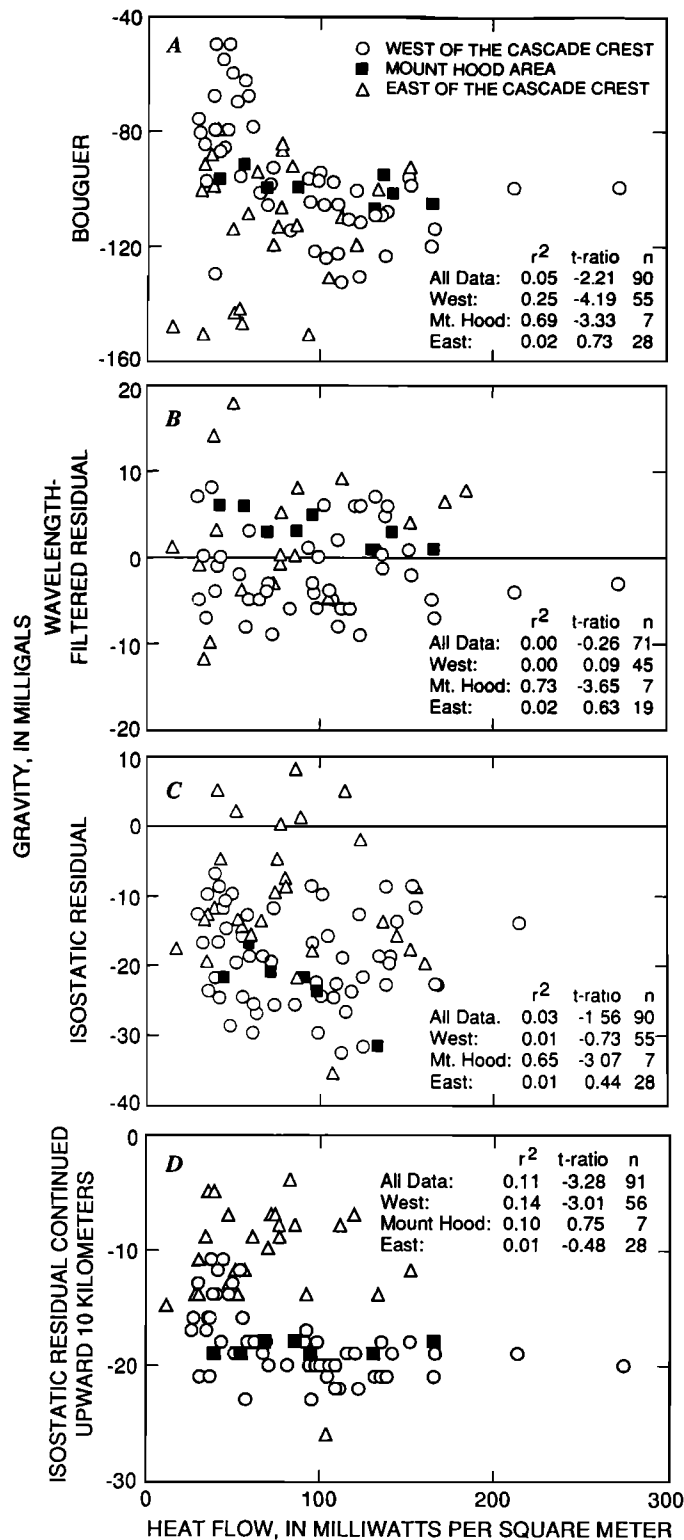


Fig. 20. Relation between heat flow and gravity data. The r^2 and t -ratio values are for linear regressions of gravity on heat flow. Heat flow data from the study area are those compiled in Ingebritsen *et al.* [1988]; holes identified as nearly isothermal or otherwise advectively disturbed were omitted, and only the better-quality heat flow estimates are used here. Bouguer gravity data (Figure 20a) are from Godson and Sckeibe [1982], wavelength-filtered residual data (Figure 20b) from Couch *et al.* [1982b], isostatic residual data (Figure 20c) from Simpson *et al.* [1986], and upward-continued isostatic residual data (Figure 20d) from R.J. Blakely (written communication, 1988).

for overlapping areas 77 km by 77 km or 155 km by 155 km, and Foote [1985] resolved source depths for 64-km by 64-km areas.

The lack of spatial resolution in the Curie-depth data makes it difficult to assess whether the Curie-depth boundaries correlate better with the areas of high near-surface heat flow or with the boundaries of the Quaternary arc. The speculative heat flow high in the northeastern part of the study area is clearly not correlated with shallow Curie depths (Figure 21). The relative degree of correspondence on the west side of the Quaternary arc is variable: in the McKenzie River area, the Curie-depth boundary is nearly coincident with the edge of the Quaternary arc, but west of Mount Jefferson it is closer to the edge of the proposed midcrustal heat source. Connard *et al.* [1983] and Foote [1985] invoked relatively recent intrusive activity to explain the shallow basal depths of magnetic sources beneath the High Cascades; they cited young volcanism and high heat flow as supporting evidence. Foote [1985] also interpreted the area of shallow basal source depth northwest of Austin Hot Springs (Figure 21) as being due to young intrusions. This latter interpretation is tenuous, because the Austin Hot Springs area is not characterized by young volcanism or by uniformly high heat flow. W.D. Stanley (written communication, 1990) suggests that the shallow Curie depth northwest of Austin Hot Springs more likely results from nonmagnetic Tertiary intrusions.

Stanley *et al.* [1989, 1990] mapped a deep-crustal electrical conductor at depths of 12-20 km in the Cascade Range. The upper boundary of this deep-crustal conductor rises near the Western Cascades-High Cascades boundary, where it becomes as shallow as ~6 km [e.g., Stanley *et al.*, 1989, Figures 3 and 6]. Stanley *et al.* [1989, 1990] interpreted this rise in the conductor as being due to shallow magma or to rising magmatic fluids concentrated in fractures associated with graben-bounding faults. West of the rise the conductor drops off steeply, to depths greater than those mapped east of the rise. Figure 21 shows where the rise in the conductor has been mapped.

If the deep-crustal conductor has geothermal significance, as Stanley *et al.* [1989, 1990] suggest, then a close correspondence between the shallowing of the conductor and high near-surface heat flow would support the midcrustal heat-source model (Figure 2b), whereas a westward drop-off of the conductor at the western edge of the Quaternary arc would be consistent with the lateral-flow model (Figure 2a). As with the Curie-depth interpretations, the relative degree of correspondence is variable. Four magnetotelluric profiles traverse the Cascade Range in the area shown in Figure 21 [Stanley *et al.*, 1989]. Along the northernmost and southernmost profiles the westward drop-off of the conductor is relatively close to the edge of the Quaternary arc; west of Mount Jefferson it lies between the Quaternary arc and the near-surface heat flow transition; and southwest of Mount Jefferson it more closely coincides with the heat flow transition.

Stanley *et al.* [1989, 1990] also evaluated seismic-refraction data from the Cascade Range. They noted that extensive magma accumulation in the middle crust is not compatible with seismic results, which show no extensive low-velocity high-attenuation regions below the Oregon Cascade Range.

The regional gravity, magnetic, and electrical geophysical data fail to distinguish between the two conceptual models depicted in Figure 2. The Bouguer and upwardly continued isostatic residual gravity data show a weak negative correlation with heat flow. However, the gravity features responsible for

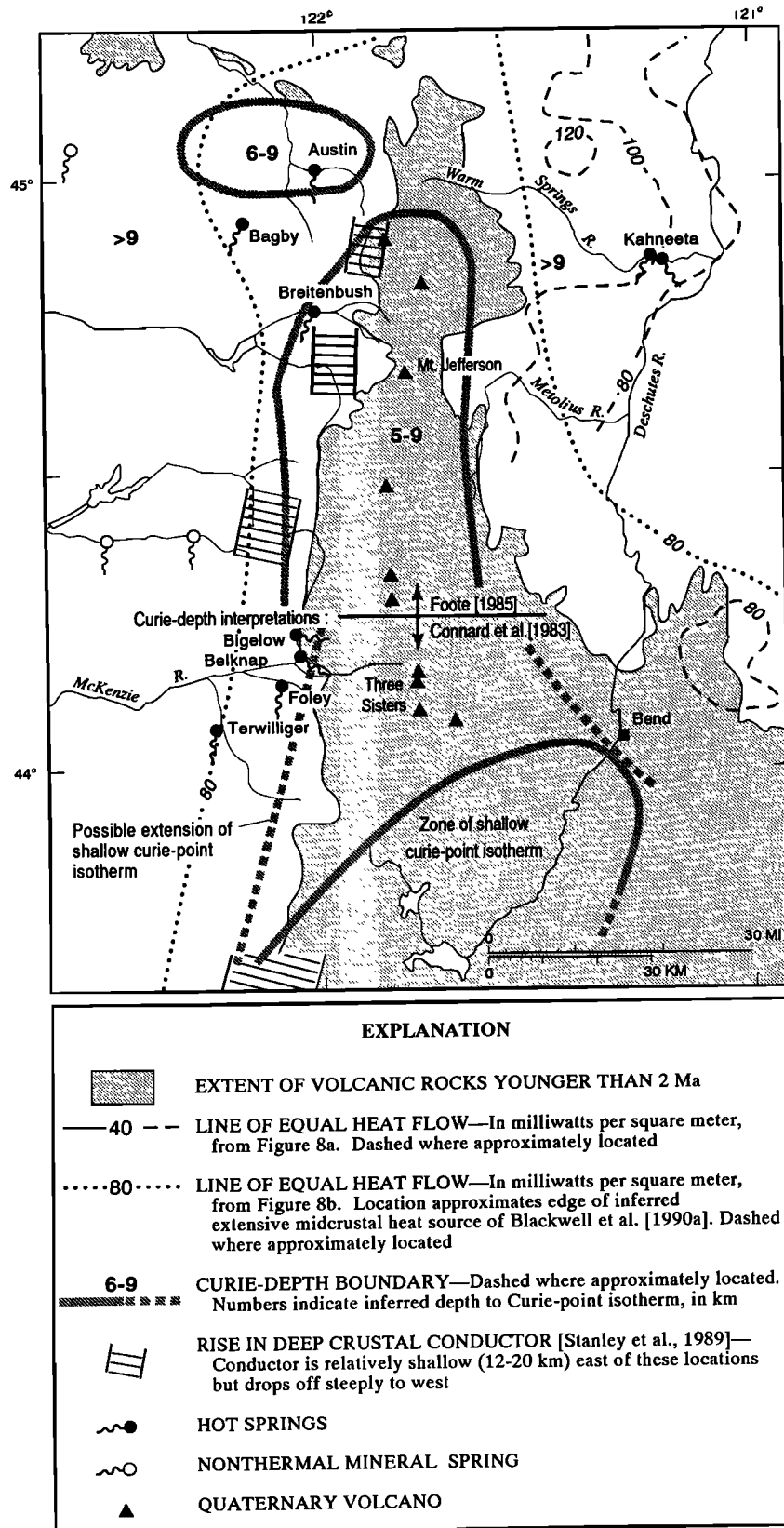


Fig. 21. Map showing relation between near-surface heat flow, Curie-depth boundaries [Connard et al., 1983; Foote, 1985], and the rise in Stanley et al.'s [1989, 1990] deep-crustal conductor. Blackwell et al.'s [1990a] 80 mW m^{-2} contour represents the inferred position of the edge of Blackwell et al.'s [1982, 1990a] midcrustal heat source. Locations of the rise in the deep-crustal conductor are from Stanley et al.'s [1989] profiles BR2, BR1, DD', and EE' (see their Figures 1 and 5 for approximate locations).

these correlations can be explained in the study area without invoking thermal effects [Blakely and Jachens, 1990], and wavelength-filtered and unsmoothed isostatic residual gravity data show no correlation with heat flow. The magnetic and electrical boundaries have variable degrees of correspondence with the boundaries expected from the alternate conceptual models. The seismic-refraction data seemingly preclude extensive magma accumulations in the middle crust, but they do not rule out small pockets of magma in the region of the proposed midcrustal heat source (Figure 2b).

COMPARISON WITH OTHER AREAS

Both in central Oregon and in southern British Columbia [Lewis et al., 1988], abrupt increases in near-surface conductive heat flow are located well seaward (west) of the active volcanic zone. A common explanation seems likely. In each case, other workers [Blackwell et al., 1982, 1990a; Lewis et al., 1988] have proposed a magmatic origin for the increase in heat flow. However, in each case the heat flow increase coincides with the major discharge area for regional groundwater flow. In Oregon the heat flow transition coincides with a belt of hot springs in the Western Cascades [e.g., Blackwell et al., 1982, Figure 8], and in British Columbia it appears to be located near the heads of fjords [Lewis et al., 1988, Figures 2 and 4] which represent the base level for groundwater flow. Systematic collection of water-chemistry data in British Columbia would help to determine whether a variant of the lateral-flow model (Figure 2a) can explain the Canadian observations.

Comparison with better-explored arcs provides some perspective on geothermal resource estimates for the central Oregon Cascade Range. The Taupo volcanic zone (TVZ) of New Zealand is petrologically and geomorphically very different from the Cascade Range: the dominantly rhyolitic eruptive products fill a broad structural and topographic depression. However, it is perhaps the only volcanic-arc segment where heat-discharge rates are as well known as in central Oregon. Table 4 compares length-normalized heat-discharge rates and resource estimates for the TVZ and central Oregon. Rates of volcanic production, volcanic heat discharge, and hydrothermal heat discharge are approximately an order of magnitude higher in the TVZ; the hydrothermal/volcanic heat-discharge ratios are similar. The New Zealand Department of Scientific and Industrial Research has estimated that the geothermal power potential of the TVZ ($6 \text{ MW}_e \text{ km}^{-1}$) amounts to about one third of the natural heat discharge ($20 \text{ MW}_e \text{ km}^{-1}$). In contrast, the power estimates of Black et al. [1983] for central Oregon (6 to $900 \text{ MW}_e \text{ km}^{-1}$) are 4 to 500 times larger than the natural heat discharge ($\sim 2 \text{ MW}_e \text{ km}^{-1}$). The relatively conservative New Zealand estimate is based on extensive research drilling and ongoing exploitation of three geothermal fields. Perhaps the published resource estimates for central Oregon are overly optimistic.

SUMMARY

The Cascade Range in central Oregon is characterized by relatively high Quaternary volcanic extrusion rates and hot-spring discharge rates and by high conductive heat flow. Extrusion rates and hot-spring discharge rates decrease both to the north and south, and conductive heat flow decreases to the north and possibly to the south. Alternate conceptual models advanced to explain the near-surface heat flow observations involve (1) a laterally extensive midcrustal heat source underlying both the

TABLE 4. Comparison of Heat Discharge and Geothermal Resource Estimates for the Central Oregon Cascade Range and the Taupo Volcanic Zone (TVZ)

	Cascades, 135 km	TVZ, 250 km
Volcanic production	3-6 $\text{km}^3/\text{m.y.}$ (basaltic andesite)	33 $\text{km}^3/\text{m.y.}$ (rhyolite)
Volcanic heat discharge	0.6 MW	4 MW
Hydrothermal heat discharge	1.1 MW	16 MW
Hydrothermal:volcanic heat discharge (ratio)	2	4
Estimated geothermal potential	6-900 MWe	6 MWe
Estimated geothermal potential: natural heat discharge (ratio)	4-500	0.3
Current geothermal power production	0	1 MWe

All rates are length-normalized. Production and heat discharge rates for the TVZ were summarized by Hedenquist [1986]. Estimates of geothermal potential are from Black et al. [1983] and Lawless et al. [1981].

Quaternary arc and adjacent older rocks and (2) a relatively narrow deep heat flow anomaly that expands laterally at shallow depths due to groundwater flow (the lateral-flow model).

All hot springs in the study area ($44^\circ 00'$ to $45^\circ 15' \text{ N}$) discharge from Miocene or Oligocene rocks at elevations of 440-680 m; there are no hot springs in the Quaternary arc. The hot springs generally occur in the deeply incised valleys of major streams that originate in the Quaternary arc. The occurrence of hot springs within a relatively narrow elevation range implies that topography is a major control on hot-spring location; most of the hot springs are also located near the surface exposures of permeable structurally or stratigraphically controlled conduits.

The isotopic composition of thermal waters in the Western Cascades is similar to that of meteoric waters at elevations of 1350-1850 m. Recharge at elevations of 1350-1850 m implies recharge within the Quaternary arc, because only very limited areas outside the Quaternary arc attain such elevations. The isotopic composition of the Western Cascade thermal waters can also be explained in terms of local recharge under colder (Pleistocene) climatic conditions. Because the Western Cascade hot springs are located at sites that would tend to capture regional groundwater flow from the Quaternary arc, we prefer to explain the isotopic composition in terms of recharge at higher elevations during the Holocene.

Commonly used geothermometers (silica, Na-K-Ca, and $\text{SO}_4\text{-H}_2\text{O}$) give disparate results when applied to the Na-Cl and Na-Ca-Cl waters of the Western Cascades. However, the $\text{SO}_4\text{-H}_2\text{O}$ isotope equilibrium and anhydrite saturation temperatures for these waters are similar, suggesting that the $\text{SO}_4\text{-H}_2\text{O}$ temperatures (136-181 $^\circ\text{C}$) are the best indicators of thermal-fluid temperatures at depth. Total advective heat transport by the hot-spring systems in the study area is $\sim 148 \text{ MW}$, which represents a significant fraction of the regional heat budget.

These observations and measurements thus suggest that gravitationally driven thermal-fluid circulation transports significant amounts of heat from the Quaternary arc into older Western Cascade rocks. This pattern of regional groundwater flow profoundly affects near-surface conductive heat flow. The Quaternary arc and adjacent 2-7-Ma volcanic rocks constitute a large area of low-to-zero near-surface conductive heat flow that results from downward and lateral flow of cold groundwater. In contrast, near-surface conductive heat flow is anomalously high where rocks older than ~7 Ma are exposed in the eastern part of the Western Cascades physiographic subprovince. The thickness of the zone of low-to-zero conductive heat flow is poorly known and presumably highly variable; it may thicken significantly beneath topographic highs.

We simulated groundwater flow and heat transport through two generalized geologic cross sections west of the Cascade Range crest: one in the Breitenbush area, where there is no evidence for major arc-parallel normal faulting, and one in the McKenzie River drainage, where major graben-bounding faults exist. Two alternate conceptual models for the thermal structure were simulated by varying the distribution of deep heat sources. The results show that either model can satisfy the near-surface thermal observations. The near-surface observations in the Breitenbush area are most readily explained in terms of lateral heat transport by regional groundwater flow. Unfortunately, given significant advective heat transport, the deep thermal structure cannot be uniquely inferred from the available data. The sparser thermal data set from the McKenzie River area can be explained either by deep regional groundwater flow or by a conduction-dominated system, with groundwater flow essentially confined to Quaternary rocks and fault zones. The simulations constrain the regional permeability structure: in order to match the heat flow observations, the bulk permeability of the youngest (<2.3 Ma) rock unit simulated must be about 10^{-14} m²; that of the oldest (>18 Ma) about 10^{-17} m².

Regional gravity, magnetic, and electrical geophysical data also presently fail to distinguish between the alternate conceptual models of the deep thermal structure. Deep drilling in the areas of high heat flow in the older rocks could indicate which model is more appropriate for the near-surface heat flow data. In such areas uniformly high conductive heat flow would be consistent with the midcrustal heat source model, and reduced heat flow below zones of active groundwater circulation would be consistent with the lateral-flow model. The data from heat flow site 61 (Figure 7) show reduced heat flow below a thermal aquifer, but the temperature profile can be matched with either a high (>100 mW m⁻²) or low (60-70 mW m⁻²) back-ground heat flow, depending on the longevity of the hydrothermal system. Quantitative data regarding the deep permeability structure are critical to an understanding of hydrothermal circulation and are essentially nonexistent. Sets of permeability tests in wells with changing temperature gradients, like that observed at heat flow site 61, would be particularly useful.

The actual thermal structure is probably more complex than either of the models discussed in this report. Careful comparison with other, better-explored arcs may prove fruitful. A comparison of length-normalized heat-discharge rates and resource estimates for the Taupo volcanic zone and central Oregon suggests that published resource estimates for central Oregon are overly optimistic.

Acknowledgments. Kari Paulson constructed the integrated-finite-difference grid used to simulate hydrothermal circulation in the McKenzie

River cross section, and Diane Cassidy derived the groundwater recharge estimates. Fred Grubb and Jack Kennelly provided logistical support for our heat flow measurements. Lynne Fahlquist provided SO₄ - H₂O temperatures for Foley and Kahneeta Springs. Peggy O'Brien Dickinson of Woods Hole Oceanographic Institution provided unpublished helium-isotope data for Austin, Bagby, and Breitenbush Hot Springs. Gerald Black and George Priest of the Oregon Department of Geology and Mineral Industries made their heat flow files available to us, and Joe Gonthier made available unpublished water-chemistry data from the Bend-Redmond area. We also thank the Confederated Tribes of the Warm Springs Reservation for cooperating and assisting with field work; Diane Cassidy, Lisa Shepherd, Milo Crumrine, Rebecca Hamon, Kari Paulson, and Richard Conroy for assistance in the field; and numerous private citizens for allowing us to sample and make measurements in their springs and wells. Rick Blakely, Hedef Essaid, Patrick Muffler, Rick Saltus, Mike Sorey, Dal Stanley, Art White, and Colin Williams provided comprehensive technical reviews of the manuscript, or portions thereof. The paper also benefited from thorough, critical reviews by JGR referees Dave Blackwell and Craig Forster. David Jones and Jeanne Dileo-Stevens drafted the figures.

REFERENCES

- Baldwin, E.M., *Geology of Oregon* (revised ed.), Kendall/Hunt, Dubuque, Iowa, 1976.
- Black, G.L., D.D. Blackwell, and J.L. Steele, Heat flow in the Oregon Cascades, in *Geology and Geothermal Resources of the Central Oregon Cascade Range, Spec. Pap. 15*, edited by G.R. Priest and B.F. Vogt, pp. 69-76, Oregon Department of Geology and Mineral Industries, Portland, 1983.
- Blackwell, D.D., and S.L. Baker, Thermal analysis of the Breitenbush geothermal system, *Geotherm. Resour. Counc. Trans.*, 12, 221-227, 1988a.
- Blackwell, D.D., and S.L. Baker, Thermal analysis of the Austin and Breitenbush geothermal systems, Western Cascades, Oregon, *Geology and geothermal resources of the Breitenbush-Austin Hot Springs area, Clackamas and Marion Counties, Oregon, Open-File Rep. O-88-5*, edited by D.R. Sherrod, pp. 47-62, Oregon Department of Geology and Mineral Industries, Portland, 1988b.
- Blackwell, D.D., and J.L. Steele, A summary of heat flow studies in the Cascade Range, *Geotherm. Resour. Counc. Trans.*, 7, 233-236, 1983.
- Blackwell, D.D., and J. L. Steele, Heat flow of the Cascade Range, Proceedings of the workshop on geothermal resources of the Cascade Range, edited by M. Guffanti and L.J.P. Muffler, *U.S. Geol. Surv. Open-File Rep. 85-521*, 20-23, 1985.
- Blackwell, D.D., and J.L. Steele, Geothermal data from deep holes in the Oregon Cascade Range, *Geotherm. Resour. Counc. Trans.*, 11, 317-322, 1987.
- Blackwell, D.D., R.G. Bowen, D.A. Hull, J. Riccio, and J.L. Steele, Heat flow, arc volcanism, and subduction in northern Oregon, *J. Geophys. Res.*, 87, 8735-8754, 1982.
- Blackwell, D.D., J.L. Steele, M.K. Frohme, C.F. Murphy, G.R. Priest, and G.L. Black, Heat flow in the Oregon Cascade Range and its correlation with regional gravity, Curie point depths, and geology, *J. Geophys. Res.*, 95, 19,475-19,494, 1990a.
- Blackwell, D.D., J.L. Steele, S. Kelley, and M.A. Korosec, Heat flow in the State of Washington and thermal conditions in the Cascade Range, *J. Geophys. Res.*, 95, 19,495-19,516, 1990b.
- Blakely, R.J., Curie temperature isotherm analysis and tectonic implications of aeromagnetic data from Nevada, *J. Geophys. Res.*, 93, 11,817-11,832, 1988.
- Blakely, R.J., and R.C. Jachens, Volcanism, isostatic residual gravity, and regional tectonic setting of the Cascade volcanic province, *J. Geophys. Res.*, 95, 19,439-19,452, 1990.
- Bodvarsson, G.S., Mathematical modeling of geothermal systems, Ph.D. thesis, University of California, Berkeley, 1982.
- Brehler, B. and R. Fuge, Chapter on Bromine, *Handbook of Geochemistry, Vol. 2(3)*, edited by K.H. Wedepohl, Springer-Verlag, New York, 1978.
- Brook, C.A., R.H. Mariner, D.R. Mabey, J.R. Swanson, M. Guffanti, and L.J.P. Muffler, Hydrothermal convection systems with reservoir temperatures >90 °C, Assessment of geothermal resources of the United States - 1978, edited by L.J.P. Muffler, *U.S. Geol. Surv. Circ. 790*, 18-85, 1979.
- Burnham, C.W., Magmas and hydrothermal fluids, *Geochemistry of Hydrothermal Ore Deposits*, edited by H.L. Barnes, John Wiley, pp. 71-136, New York, 1979.

- Callaghan, E., Some features of the volcanic sequence in the Cascade Range in Oregon, *Eos Trans. AGU 14th Annual Meeting*, 243-249, 1933.
- Callaghan, E., and A.F. Buddington, Metalliferous mineral deposits of the Cascade Range in Oregon, *U.S. Geol. Surv. Bull.* 893, 1938.
- Connard, G., R. Couch, and M. Gemperle, Analysis of aeromagnetic measurements from the Cascade Range in central Oregon, *Geophysics*, 48, 376-390, 1983.
- Conrey, R.M., and D.R. Sherrod, Stratigraphy of drill holes and geochemistry of surface rocks, Breitenbush Hot Springs 15-minute quadrangle, Cascade Range, Oregon, in *Geology and Geothermal Resources of the Breitenbush-Austin Hot Springs Area, Clackamas and Marion Counties, Oregon, Open-File Rep. O-88-5*, edited by D.R. Sherrod, pp. 15-29, Oregon Department of Geology and Mineral Industries, Portland, 1988.
- Couch, R.W., G.S. Pitts, M. Gemperle, D.E. Braman, and C.A. Veen, Gravity anomalies in the Cascade Range in Oregon: structural and thermal implications, *Open-File Rep. O-82-9*, Oregon Department of Geology and Mineral Industries, Portland, 1982a.
- Couch, R.W., G.S. Pitts, M. Gemperle, C.A. Veen, and D.E. Braman, Residual gravity maps, northern, central, and southern Oregon Cascade Range, Oregon, *Geological Map Series GMS-26*, scale 1:250,000, Department of Geology and Mineral Industries, Portland, 1982b.
- Dansgaard, W., Stable isotopes in precipitation, *Tellus*, 16, 436-468, 1964.
- Ellis, A.J., and W.A.J. Mahon, *Chemistry and Geothermal Systems*, Academic, San Diego, Calif., 1977.
- Foote, R.W., Curie-point isotherm mapping and interpretation from aeromagnetic measurements in the northern Oregon Cascades, M.S. thesis, Oregon State University, Corvallis, 1985.
- Forster, C., and L. Smith, Groundwater flow systems in mountainous terrain. 2, Controlling factors, *Water Resour. Res.*, 24, 1011-1023, 1988.
- Fournier, R.O., Application of water chemistry to geothermal exploration and reservoir engineering, *Geothermal Systems: Principles and Case Histories*, edited by L. Rybach and L.J.P. Muffler, pp. 109-143, John Wiley, New York, 1981.
- Fournier, R.O., and J.J. Rowe, Estimation of underground temperatures from the silica content of water from hot springs and wet-steam wells, *Am. J. Sci.*, 264, 685-697, 1966.
- Fournier, R.O., and A.H. Truesdell, An empirical Na-K-Ca geothermometer for natural waters, *Geochim. Cosmochim. Acta*, 37, 1255-1275, 1973.
- Frank, F.J., Ground water in the Myrtle Creek-Glendale area, Douglas County, Oregon, *U.S. Geol. Surv. Water Resour. Invest.*, 79-8, scale 1:62,500, 1979.
- Gat, J.R., The isotopes of hydrogen and oxygen in precipitation, *Handbook of Environmental Isotope Geochemistry, Vol. 1*, edited by P. Fritz and J.Ch. Fontes, pp. 21-47, Elsevier, New York, 1980.
- Godson, R.H., and D.M. Scheibe, Description of magnetic tape containing conterminous U.S. gravity data in gridded format, *Rep. PB-254798*, Nat. Tech. Inf. Serv. Rep., Springfield, Va., 1982.
- Hamilton, W., and W.B. Myers, Cenozoic tectonics of the western United States, *Rev. Geophys.*, 4, 509-549, 1966.
- Hardie, L.A., Origin of CaCl₂ brines by basalt-seawater interaction: Insights provided by some simple mass balance calculations, *Contrib. Mineral. Petrol.*, 82, 205-213, 1983.
- Harris, P.G., W.Q. Kennedy, and C.M. Scarfe, Volcanism versus plutonism - the effect of chemical composition, in *Mechanism of Igneous Intrusion, Geol. J. London Spec. Issue no. 2*, edited by G. Newall and N. Rast, pp. 187-200, University of Liverpool, Liverpool, England, 1970.
- Hedenquist, J.W., Geothermal systems in the Taupo volcanic zone: their characteristics and relation to volcanism and mineralisation, Late Cenozoic volcanism in New Zealand, edited by I.E.M. Smith, *Bull. R. Soc. N.Z.*, 23, 134-168, 1986.
- Ingebritsen, S.E., and M.L. Sorey, A quantitative analysis of the Lassen hydrothermal system, north central California, *Water Resour. Res.*, 21, 853-868, 1985.
- Ingebritsen, S.E., R.H. Mariner, D.E. Cassidy, L.D. Shepherd, T.S. Presser, M.K.W. Pringle, and L.D. White, Heat-flow and water-chemistry data from the Cascade Range and adjacent areas in north-central Oregon, *U.S. Geol. Surv. Open File Rep.*, 88-702, 1988.
- Ingebritsen, S.E., D.R. Sherrod, and R.H. Mariner, Heat flow and hydrothermal circulation in the Cascade Range, north-central Oregon, *Science*, 243, 1458-1462, 1989.
- Ingebritsen, S.E., R.H. Mariner, and D.R. Sherrod, Hydrothermal systems of the Cascade Range, north-central Oregon, *U.S. Geol. Surv. Open File Rep.*, 91-69, 1991 (Also, *U.S. Geol. Surv. Prof. Pap.*, 1044-L, in press, 1992.)
- Jaeger, J.C., Thermal effects of intrusions, *Rev. Geophys.*, 2, 443-466, 1964.
- Keith, T.E.C. Hydrothermal alteration patterns in the Breitenbush Hot Springs area, Cascade Range, Oregon, *Geotherm. Resour. Coun. Trans.*, 12, 299-304, 1988.
- Lawless, J.V., J.T. Lumb, L. Clelland, D. Kear, and S.R. Drew, Geothermal energy for New Zealand's future, *DSIR Bull.*, 229, 1981.
- Lewis, T.J., W.H. Bentkowski, E.E. Davis, R.D. Hyndman, J.G. Souther, and J.A. Wright, Subduction of the Juan de Fuca plate: thermal consequences, *J. Geophys. Res.*, 93, 15,207-15,225, 1988.
- Mariner, R.H., T.S. Presser, and W.C. Evans, Hot springs of the central Sierra Nevada, California, *U.S. Geol. Surv. Open File Rep.*, 77-559, 1977.
- Mariner, R.H., T.S. Presser, W.C. Evans, and M.K.W. Pringle, Discharge rates of thermal fluids in the Cascade Range of Oregon and Washington and their relationship to the geologic environment, Proceedings of work-shop XLIV: Geological, geophysical, and tectonic setting of the Cascade Range, edited by L.J.P. Muffler, C.S. Weaver, and D.D. Blackwell, *U.S. Geol. Surv. Open File Rep.* 89-178, 663-694, 1989.
- Mariner, R.H., J.R. Swanson, G.J. Orris, T.S. Presser, and W.C. Evans, Chemical and isotopic data for water from thermal springs and wells of Oregon, *U.S. Geol. Surv. Open File Rep.*, 80-737, 1980.
- Mariner, R.H., T.S. Presser, W.C. Evans, and M.K.W. Pringle, Discharge rates of fluid and heat by thermal springs of the Cascade Range, Washington, Oregon, and northern California, *J. Geophys. Res.*, 95, 19,517-19,532, 1990.
- Mase, C.W., J.H. Sass, A.H. Lachenbruch, and R.J. Munroe, Preliminary heat-flow investigations of the California Cascades, *U.S. Geol. Surv. Open File Rep.*, 82-150, 1982.
- McFarland, W.D., A description of aquifer units in western Oregon, *U.S. Geol. Surv. Open File Rep.*, 82-165, 1982.
- McKenzie, W.F., and A.H. Truesdell, Geothermal reservoir temperatures estimated from the oxygen isotope compositions of dissolved sulfate and water from hot springs and shallow drillholes, *Geothermics*, 5, 51-61, 1977.
- Mizutani, Y., and T.A. Rafter, Oxygen isotopic composition of sulphates - part 3. Oxygen isotopic fractionation in the bisulfate ion-water system, *N. Z. J. Sci.*, 12, 54-59, 1969.
- Priest, G.R., Geothermal exploration in Oregon, 1984, *Oreg. Geol.*, 47, 63-66, 1985.
- Priest, G.R., N.M. Woller, and M.L. Ferns, Geologic map of the Breitenbush River area, Linn and Marion Counties, Oregon, *Geological Map Series GMS-46*, scale 1:62,500, Oregon Department of Geology and Mineral Industries, Portland, 1987.
- Priest, G.R., G.L. Black, N.M. Woller, and E.M. Taylor, Geologic map of the McKenzie Bridge quadrangle, Lane County, Oregon, *Geological Map Series GMS-28*, scale 1:62,500, Oregon Department of Geology and Mineral Industries, Portland, 1988.
- Robison, J.H., Availability and quality of ground water in the Sutherlin area, Douglas County, Oregon, *U.S. Geol. Surv. Water Resour. Invest.*, 74-32, scale 1:62,500, 1974.
- Robison, J.H., and C.A. Collins, Availability and quality of ground water in the Drain-Yoncalla area, Douglas County, Oregon, *U.S. Geol. Surv. Water Resour. Invest.*, 76-105, scale 1:62,500, 1977.
- Sherrod, D.R., Geology, petrology, and volcanic history of a portion of the Cascade Range between latitudes 43° -44° N, central Oregon, U.S.A., Ph.D. thesis, University of California, Santa Barbara, 1986.
- Sherrod, D.R., and J.G. Smith, Preliminary map of upper Eocene to Holocene volcanic and related rocks of the Cascade Range, Oregon, *U.S. Geol. Surv. Open File Rep.*, 89-14, scale 1:500,000, 1989.
- Sherrod, D.R., and J.G. Smith, Quaternary extrusion rates of the Cascade Range, north-western United States and southern British Columbia, *J. Geophys. Res.*, 95, 19,465-19,474, 1990.

S.E. Ingebritsen and R.H. Mariner, U.S. Geological Survey, Mail Stop 439, 345 Middlefield Road, Menlo Park, CA 94025.
D.R. Sherrod, U.S. Geological Survey, Vancouver, WA 98661.

(Received May 13, 1991;
revised November 8, 1991;
accepted December 10, 1991.)